THE UNIVERSITY OF QUEENSLAND

AUSTRALIA

Development of anti-PEG bispecific antibodies for targeting PEGylated nanoparticles to tumour cells

Tim Ruder

BBiomed. Sc.; Hons.

A thesis submitted for the degree of Master of Philosophy at

The University of Queensland in 2017

Australian Instititute for Bioengineering and Nanotechnology

Thesis Abstract

Cancer treatment is significantly impaired by the low therapeutic index traditionally exhibited by most current chemotherapeutics. This is principally a result of a ubiquitous systemic distribution of these drugs. Recent advances in chemotherapy have seen the development of both antibody conjugated chemotherapeutics and drug conjugated nanoparticles each with their own unique advantages and drawbacks. However, to date, there are no approved targeted nanoparticles. Of the seven FDA approved nanoparticles two are entirely composed of polyethylene glycol (PEG) or are surface PEGylated. Other FDA approved nanoparticles would likely benefit from PEGylation to diminish aggregation and increase circulation time. In this study, we designed bispecific antibodies targeting both a PEG chain on a nanoparticle and cancer-associated cell surface targets. Our initial bispecific antibody designs yielded one bispecific antibody that successfully binds both the PEG nanoparticle and the epidermal growth factor receptor (EGFR) antigen on cancer cells. Capture ELISA showed the affinity of the anti-PEG component to be comparable to the parent monoclonal antibody. We further show that these bispecific antibodies bind to EGFR overexpressing MDA MB 468 cells both *in vitro* and *in vivo*.

Declaration by author

This thesis is composed of my original work and contains no material previously published or written by another person except where due reference has been made in the text. I have clearly stated the contribution by others to jointly-authored works that I have included in my thesis.

I have clearly stated the contribution of others to my thesis as a whole, including statistical assistance, survey design, data analysis, significant technical procedures, professional editorial advice, and any other original research work used or reported in my thesis. The content of my thesis is the result of work I have carried out since the commencement of my research higher degree candidature and does not include a substantial part of work that has been submitted to qualify for the award of any other degree or diploma in any university or other tertiary institution. I have clearly stated which parts of my thesis, if any, have been submitted to qualify for another award.

I acknowledge that an electronic copy of my thesis must be lodged with the University Library and, subject to the policy and procedures of The University of Queensland, the thesis be made available for research and study in accordance with the Copyright Act 1968 unless a period of embargo has been approved by the Dean of the Graduate School.

I acknowledge that copyright of all material contained in my thesis resides with the copyright holder(s) of that material. Where appropriate I have obtained copyright permission from the copyright holder to reproduce material in this thesis.

Publications during candidature

Howard CB, Fletcher N, Houston ZH, Fuchs AV, Boase NR, Simpson JD, Raftery LJ, Ruder T, Jones ML, de Bakker CJ, Mahler SM. Overcoming Instability of Antibody-Nanomaterial Conjugates: Next Generation Targeted Nanomedicines Using Bispecific Antibodies. *Adv Healthc Mater*. 2016 Aug;5(16):2055-68. doi: 10.1002/adhm.201600263. Epub 2016 Jun 10.

Publications included in this thesis

No publications included

Contributions by others to the thesis

In Vivo Fluorescent Imaging conducted by Nicholas Fletcher; Thurecht Group.

Statement of parts of the thesis submitted to qualify for the award of another degree

None

Acknowledgements

"Sed ut perspiciatis unde omnis iste natus error sit voluptatem accusantium doloremque laudantium, totam rem aperiam, eaque ipsa quae ab illo inventore veritatis et quasi architecto beatae vitae dicta sunt explicabo. Nemo enim ipsam voluptatem quia voluptas sit aspernatur aut odit aut fugit, sed quia consequuntur magni dolores eos qui ratione voluptatem sequi nesciunt. Neque porro quisquam est, qui dolorem ipsum quia dolor sit amet, consectetur, adipisci velit, sed quia non numquam eius modi tempora incidunt ut labore et dolore magnam aliquam quaerat voluptatem. Ut enim ad minima veniam, quis nostrum exercitationem ullam corporis suscipit laboriosam, nisi ut aliquid ex ea commodi consequatur? Quis autem vel eum iure reprehenderit qui in ea voluptate velit esse quam nihil molestiae consequatur, vel illum qui dolorem eum fugiat quo voluptas nulla pariatur?

At vero eos et accusamus et iusto odio dignissimos ducimus qui blanditiis praesentium voluptatum deleniti atque corrupti quos dolores et quas molestias excepturi sint occaecati cupiditate non provident, similique sunt in culpa qui officia deserunt mollitia animi, id est laborum et dolorum fuga. Et harum quidem rerum facilis est et expedita distinctio. Nam libero tempore, cum soluta nobis est eligendi optio cumque nihil impedit quo minus id quod maxime placeat facere possimus, omnis voluptas assumenda est, omnis dolor repellendus. Temporibus autem quibusdam et aut officiis debitis aut rerum necessitatibus saepe eveniet ut et voluptates repudiandae sint et molestiae non recusandae. Itaque earum rerum hic tenetur a sapiente delectus, ut aut reiciendis voluptatibus maiores alias consequatur aut perferendis doloribus asperiores repellat."

- Cicero

Gratias vobis ago omnibus habentibus contulit thesi.

Per aspera ad astra.

Keywords

cd171, cd200, egfr, nanoparticle, bsab mediated targeting

Australian and New Zealand Standard Research Classifications (ANZSRC)

ANZSRC code: 090399, Biomedical Engineering, 100%

Fields of Research (FoR) Classification

0903 Biomedical Engineering, 100%

Table of Contents

Chapter 1: Introduction and Background

Clinical outcomes of current cancer therapy are significantly impacted by the lack of tumour specificity of current diagnostic and therapeutic treatments (Langer et al. 2001). A lack of specificity will impair the collection of meaningful imaging data crucial to early diagnosis and staging of cancers. During chemotherapy, a lack of specific targeting will directly result in the destruction of all rapidly proliferating cells and is responsible for the significant side effects of chemotherapy. Low specificity is also complicit in tumour resistance to chemotherapeutic drugs as insufficient amounts of drug reach the tumour. Thus increasing the chance of resistance to the chemotherapeutic and increasing the cost of cancer treatment (Gerber 2008). Numerous approaches have been explored in engineering alternative approaches to cancer therapy. Currently, the most promising strategies involve the development of novel, inert, nanoparticles as well as the generation of novel antibodies targeting antigens which do not commonly illicit an immune response and thus have no natural antibodies (Yoo et al. 2011, Burden et al. 2012). Other approaches to cancer therapy include the use of radiolabeled or drug conjugated antibodies as well as novel antibody formats such as bispecific antibodies (BsAbs) which allow for the targeting of multiple antigens. The Fc region often utilized for drug conjugation is the key region used for immune signalling by antibodies and has been shown to be highly immunogenic. This diminishes circulation time and poses the risk of infusion reactions ranging from mild reactions, such as flushing, to lethal anaphylactic shock (Meisel 2011). The fragment crystallizable (Fc) receptors FcyRIIA and FcyRIIB have also been shown to induce anaphylactic shock in response to antigen binding (Joensson et al. 2012). Furthermore payload delivery per antibody is relatively low. Fc linked drug is also exposed to enzymes, which prevents the use of unstable drug compounds such as siRNA, and may show activity whilst still linked to the Fc, thus exhibiting systemic toxicity en route to the target. A phase I clinical trial investigating the tolerance towards a drug conjugated to a single chain variable fragment (scFv), containing no Fc region, found no evidence of infusion reaction (Von Minckwitz et al. 2005) and showed none of the hepatotoxicity that was displayed when the full monoclonal antibody drug conjugate was injected.

1.1 Nanoparticles in Cancer Diagnosis and Therapy

Recent innovations in cancer research have seen the development of a large variety of nanoparticles some of which are currently undergoing clinical trials (Sanna et al. 2014). These nanoparticles feature material properties which enhance their delivery to the tumour and can deliver vast payloads of a drug with only a single Nanoparticle. Nanoparticles have been shown to be capable of carrying payloads ranging from siRNA (Wang et al. 2014) to proteinaceous cytotoxins (Pan et al. 2011) and low molecular weight drugs

commonly utilized in chemotherapy. This may, in the future, offer hope to patients suffering from drug-resistant tumours as drug resistance genes, or possibly even oncogenes, can be knocked out with siRNA treatment. The key advantages of nanoparticles are that they both protect the drug from inactivation whilst en route to the target as well as prevent unwanted activity of drug whilst en route to the target and preventing the severe side effects usually associated with untargeted drug delivery. Nanoparticles currently in development include dendrimers, liposomes, polymeric particles, micelles, protein cages, ceramic particles, metallic nanoparticles and functionalized carbon nanotubes (Byrne 2008). Untargeted nanoparticles, including the FDA, approved Doxil, accumulate within tumours due to the enhanced permeability and retention (EPR) effect at tumour sites, and may release their active compounds due to a time delay mechanism, degradation of the nanoparticle or linker following internalization (Firer 2013, Goodall et al. 2014, Sanna et al. 2014). These same principles also allow for the use of labelled nanoparticles as a means to conduct cancer imaging, this allows for the collection of important information regarding the staging of cancer. However, EPR is only effective once a solid tumour has formed. Other nanoparticles incorporate fluorophores as well as a chemotherapeutic drug into their composition or may be linked to radioisotopes and as such have both diagnostic as well as therapeutic applications and are referred to as theranostic applications.

1.2 Conjugation of Antibodies and Nanoparticles

To combat problems relating to the passive targeting of nanoparticles attempts have been made to conjugate monoclonal antibodies to nanoparticles (Arruebo et al. 2009). This seeks to combine the exquisite specificity of the monoclonal antibody with the vast payload of the nanoparticles and eliminates the need for a reactive nanoparticle surface. Chemical conjugation is commonly achieved using maleimide, N-hydroxysuccinimide (NHS), halo acetyl or isothiocyanate linkers. The conjugation of antibody to nanoparticles is often problematic as precise conjugation is difficult to control and can interfere with the conjugation of drug to the nanoparticle or vice versa. Reactions often require further purification and are of heterogeneous composition. In the production of BsAbs chemical crosslinking with bis-maleimide has even been associated with antibody inactivation (Ellerman 2011). This is likely a result of linker chemicals binding in binding sites of antibodies leading to inactivation due to steric hindrance. Furthermore, the introduction of Fc from monoclonal antibodies has been shown to result in a reduction in circulation time and an increase in phagocytic response. This shortcoming could be resolved by the conjugation of antibody fragments (Fragment antigen-binding (Fab) or scFv) to nanoparticles. An approach to circumvent the complications associated with the conjugation of

antibodies to nanoparticles is to use BsAbs with an affinity for both the nanoparticle as well as a cell surface target.

1.3 Bispecific Antibodies

BsAbs are engineered to bind two distinct targets and have been used in a variety of different formats (Spiess et al. 2015). BsAb designs commonly focus on forcing pairing of two different heavy chains in order to achieve dual specificity, as seen in knobs-into-holes and Dock-and-Lock methodologies (Kontermann 2012). For application relying on the presence of a Fc region, this is a good approach as it allows redirection of the immune system to and subsequent killing of a target cell. In applications where the Fc region is not required, a tandem scFv design allows for a simpler and more stable construct (Taylor et al. 2015). G4S linkers have been widely used in the production of tandem scFv BsAbs over other linkers as they give the molecule an innate flexibility correlated with the number of G4S repeats and have a low impact on the secondary structure of the neighbouring scFvs (Hollinger & Hudson 2005, Brischwein et al. 2006). This design also eliminates the Fc region from the targeting system which may aid in preserving the low immune visibility of the nanoparticle. By targeting multiple cell surface targets simultaneously higher, than otherwise possible, avidity binding may be promoted due to the close proximity of the target antigens on the cell surface.

1.4 Targeting of PEG nanoparticles to Cell surface Targets utilizing BsAbs

Tandem scFv BsAbs have previously been shown by our group to allow for the targeting of nanoparticles coated with lipopolysaccharide (LPS) to EGFR overexpressing cancer cells (Taylor et al 2015). In this study, one arm of the BsAb binds the nanoparticle and the other a cell surface target. When adsorbed to cell surfaces via BsAb, LPS coated nanoparticles have been shown to readily internalize despite their large size (Taylor et al. 2015). Nanoparticles are commonly coated with PEG in order to prevent aggregation, decrease immune visibility and increase circulation time. However, an unintended consequence of PEGylation is a poor cellular uptake of the nanoparticle as adsorption to the cell surface is diminished. The discovery of anti-PEG antibodies (Chen et al. 2012, Coles et al 2013) presents a unique opportunity to explore the use of a tandem scFv BsAb to confer an active targeting mechanism to an otherwise passively targeted nanoparticle (provided by Thurecht group) and to overcome the drawbacks associated with PEGylation.

We propose to utilize a tandem scFv BsAb consisting of 2 scFvs fused by a G4S linker in order to facilitate targeting of PEG nanoparticles toward EGFR overexpressed on tumour cells. This design

eliminates the Fc region from the targeting system and should yield a lower immune visibility of the nanoparticle than in other designs incorporating Fc regions. The conjugation of the BsAb to the PEG nanoparticle simply requires the co-incubation of the nanoparticle and BsAb in a relevant buffer (Appendix A: Figure 1). This is a considerably less complex and costly approach than chemical conjugation and avoids the numerous complications and pitfalls associated therewith. The use of BsAbs also facilitates the targeting of PEG nanoparticles to multiple targets simultaneously, by incorporating multiple BsAbs, which may again increase specificity. The use of PEG nanoparticles, in turn, may widen the therapeutic window sufficiently for the use of a larger variety of chemotherapeutics of both lower and higher potency than usual as both quantity as well as the proportion of the chemotherapeutic delivered to the tumour is significantly increased.

Given the enormous potential of targeted PEG nanoparticles, the aim of this research project is to develop a number of BsAbs, one head of which targets the nanoparticle, whilst the other will target suitable cell surface markers for use in both imaging and cancer therapy. This will be achieved by attaining the following objectives:

Objective 1: Screen of published anti-PEG monoclonal antibodies for efficacy in the tandem scFv BsAb format in combination with the previously validated anti-EGFR scFv.

Objective 2: Design and evaluate BsAbs with a range of cell surface targets for their suitability in targeting nanoparticle to tumour cells by screening in vitro and in vivo.

Chapter 2: Methods

2.1.1 BsAb Design:

Initial BsAb designs focussed principally on establishing whether existing monoclonal antibodies retained their affinity to PEG when redesigned as scFv and used within a BsAb format. To test this, we identified the heavy chain variable (VH) and light chain variable (VL) regions of sequences from published anti-PEG monoclonal antibodies (Chen et al 2012) to design an anti-PEG scFv and linked them to a Panitumumab (Jakobovits et al. 2001) scFv to make a tandem scFv BsAb using a G4S linker. Panitumumab was chosen because it is a well-characterized anti-EGFR monoclonal antibody and it was previously described as functional and stable in the scFv format (Taylor et al. 2015). EGFR is overexpressed in a large proportion of tumour cells, and as such EGFR was an ideal candidate as cell

lines were readily available and the antibody's function is well characterized. A total of 5 anti-EGFR-PEG BsAb genes were synthesized. The anti-PEG antibodies AGP 3 and 15-2 were regarded as the ones with the most potential, as they had both been described as having an affinity toward both PEG and methoxyl-PEG. ScFvs were designed by linking the heavy and light variable chains of a monoclonal antibody using a 3G4S linker. The scFvs were joined via a G4S linker to make a tandem scFv BsAb. A mammalian leader sequence, a 6xHis epitope at the N-terminal of the BsAb and a c-myc epitope at the C-terminal of the gene were incorporated in the gene design to facilitate BsAb secretion, purification, and detection. Tandem scFv BsAb genes (Appendix A: Figure 2) were synthesised by Geneart (Life Tech) with sequence codon optimisation for expression in Chinese hamster ovary (CHO) cells.

2.1.2 Cloning:

All plasmids were then re-cloned into the mammalian expression vector NBF 347, designed in-house at the National Biologics Facility (NBF) (Appendix A: Figure 3) using Hind III and NotI. The expression vectors utilised a CMV promoter upstream of the BsAb gene for expression.

2.1.2.1 Restriction digest:

BsAb genes were synthesised by Geneart, in plasmids containing Ampicillin resistance as well as NotI and HindIII restriction sites on either side of the gene. Plasmids were then resuspended in 50µl souble distilled (DDW). An aliquot of 16µl was restricted using NotI-HF (1 µl, 10000 U/µl), and HindIII (1 µl, 10000 U/µl) in 2 µl 10x cutsmart buffer. Gene inserts were purified utilizing 1% agarose gel, stained with syber safe at 100 V for 15 min. The appropriate band was then excised on a UV transilluminator. The gene insert was purified from the gel using a PCR/Gel cleanup kit (Bioline), following the manufacturer's directions.

2.1.2.2 Ligation:

Gene inserts were ligated into HindIII - NotI cut, NBF plasmid 347 containing Kanamycin resistance, using the Rapid DNA ligation kit (Roche) and ligated for 60 min according to the manufacturer's directions.

2.1.2.3 Transformation and Subcloning:

Chemically competent *E.coli* were thawed on ice. 25 µl of *E.coli* were then transformed with 2 µl ligation reaction by incubation on ice for 5 min, followed by 1 minute at 42 °C and subsequently 2 minutes on

ice. Cells were allowed to recover by addition of 250 µl LB broth was added to the reaction and incubation at 37 °C for 1 hr. Cells were screened by plating 50 µl on an LB+30 µg/ml kanamycin plate and incubating at 37°C overnight. 2 colonies were picked, inoculated into 10ml of LB + 30µg/ml kanamycin and incubated at 37 °C at 220 rpm overnight. Plasmid was then extracted from 5 ml of culture using a PureLink Quick Plasmid Miniprep kit (Invitrogen) following the manufacturer's directions. The plasmid was then checked using a restriction digest and agarose gel. 500ml of LB + 30µg/L kanamycin was inoculated with the remaining 5ml of culture and incubated overnight (8-16 hrs). Plasmid was extracted using a Maxiprep kit (Bioline) following the manufacturers' direction.

2.1.3 Transfection and Expression:

Following cloning, several ratios of DNA to PEI were trialled to optimise transfection efficiency and expression of the BsAb (Data not shown). All CHO cell expressions of BsAbs were carried out in serum free conditions. CHO cells were cultured from frozen stocks to a density of 4 x 10^6 cells/ml in 300ml of CD-CHO medium (Gibco) with 8mM Glutamax (Gibco) at 37.8 °C , 7.5% CO_2, 130 rpm, 70% humidity. The culture was subsequently pelleted at 200xg and resuspended in fresh CD-CHO medium. 600µg of DNA and 3ml of 1mg/ml 25kDa PEI were added to 12 ml of Optipro transfection medium (Gibco), to give a DNA:PEI ratio of 1:5, and incubated for 15 minutes at room temperature. Following incubation the reaction was then directly added to the culture and incubated for 4hrs at 37.8 °C, 7.5% CO2, 130rpm, 70% humidity. After incubation, the culture was fed with 70 ml (7.5%) CD CHO Efficient Feed A (Gibco), 70 ml CD (7.5%) CHO Efficient Feed B (Gibco), and 460ml CD CHO + 8mM Glutamax. The culture was then split evenly across 3 1 L conical flasks and incubated at 32 °C, 7.5%CO2, 130rpm, 70% humidity. Cell supernatant was collected at a time point (Days 10-14) when cell viability was reduced to 50%, and centrifuged at 10000xg to remove cells.

2.1.4 Purification

Cell supernatant was filtered using a 0.22 um bowman's capsule and the pH was adjusted to 6.8 - 7.3 using NaOH and HCl. BsAb was purified from cell culture supernatant using protein L and His based affinity chromatography. Hi-Traps rely on the affinity of the His-tag in the BsAb to metal Ions in the affinity column, whilst Protein L purification relies on the capture of kappa variable light chains. The supernatant was then loaded onto a 5ml Hi-Trap column at 5ml/min (GE Lifesciences) 0.5M NaOH was used for sanitation, 500 mM Imidazole (pH 7.3) was used for elution and PBS (pH 7.3) was used for all

wash and equilibration steps. Following elution from the Hi-Trap column, the sample was loaded onto a Protein L column at 5ml/min (GE Lifesciences) for further purification. 0.01 M NaOH was used for sanitation, 0.1M Glycine (pH 3) was used for elution and PBS (pH7.3) for all wash and equilibration steps. The protein peak was collected and desalted, the concentration was determined using nanodrop (Nanodrop 2000 A280).

2.1.5 SDS-PAGE Electrophoresis:

BsAb purity was assayed using sodium dodecyl sulphate polyacrylamide gel electrophoresis (SDS-PAGE), 1µl Nupage (Invitrogen) reducing agent and 2 µl Nupage sample loading buffer were added to 8µl sample and incubated at 95 °C for 3 min, samples were then loaded onto a precast 4-12% Bis-Trisacrylamide gel (and run for 30 minutes at a constant voltage of 200 V with maximum amperage of 400 mA. Gels were then rinsed with MilliQ water, stained for 24 hours using safe stain (Thermo Fisher) and subsequently destained using MilliQ water. Gels were then imaged with a Biorad Gel Doc System.

2.1.6 Purity analysis using High-Performance Liquid Chromatography:

To investigate ratios of monomer to multimer and aggregate 50 µl of 100µg/ml BsAb in PBS was loaded onto a Tosoh Biosciences TSKGel G3000SWXL size exclusion high-performance liquid chromatography (SEHPLC) column. The sample was then eluted from the column using 20% Ethanol in PBS with a flow rate of 0.5ml/min for 35 minutes and absorbance was read in-line at 215 and 280 nm.

2.1.7 Spherical molecular size and aggregation analysis using Dynamic Light Scatter:

BsAb spherical molecular size and aggregation state was determined by dynamic light scatter (DLS) utilizing a Malvern Zetasizer Nano with a backscatter angle of 173 degrees. Samples were diluted to 1mg/ml in 0.1M Arginine 0.5M NaCl Buffer with a viscosity of 0.9286 mPa/s and a refractive index of 1.349 at a temperature of 25 °C, the sample was run as a protein sample with a refractive index 1.450 and an absorbance 0.001. All measurements were taken in triplicate with a minimum of 10 reads per measurement. Following initial measurements of BsAb Nanoparticle was gradually added to the BsAb at concentrations of 1, 10 and 100 µg/ml samples were left to incubate for 15 minutes at 25 degrees and the re-assayed. Data was analyzed using Malvern Instruments Zetasizer Software v7.01

2.1.8 Initial Affinity Screening and EC50 approximation by Enzyme-Linked Immunosorbent Assay:

Enzyme-linked immunosorbent assays were (ELISA) employed in order to establish initial functionality of BsAbs as well as construct dose-response curves to establish approximate EC50 values for BsAbs

Affinity Screening:

Plates were coated with 10μg/ml PEG nanoparticle. After 12 hours at 4 °C, the plates were washed 3 times with PBS (Lonza) and blocked with 200μl 5% skim milk in PBS. After 2 hours, plates were washed 3 times with PBS, then 50μl of antibody at a concentration of 100μg/ml was added to the wells and incubated for 2 hours. Tween20 and PEG are structurally quite similar, as such protocols with and without tween20 were used concurrently. Plates were washed 5 times with PBS for a tween free protocol, or thrice with PBS 0.05% tween and twice with PBS. Antibody binding was detected using 50μl of anti-c-myc-hrp antibody at 1:5000 dilution in 5% skim milk for 1 hour. Plates were subsequently washed 8 times with PBS for the tween free protocol or 6 times with PBS-T and 2 times with PBS. 100μl TMB was the added to the wells and incubated for 10 minutes in the dark. HRP was then inactivated using 100 μl H_2SO_4 and absorbance was read on a Specramax plate reader at 450 nm.

EC50:

Plates were coated with 10μg/ml PEG nanoparticle. After 12 hours at 4°C, the plates were washed 3 times with PBS (Lonza) and blocked with 200μl 5% skim milk in PBS. After 2 hours, plates were 3 times washed with PBS, then 50 μl of antibody, ranging from 300μg/ml to 0ng/ml, were added to the plate to give a concentration curve. Following 2 hours of incubation, plates were washed 5 times with PBS for a Tween free protocol, or thrice with PBS 0.05% tween and twice with PBS. Antibody binding was detected using 50μl of anti-c-myc-hrp antibody at 1:1000 dilution in 5% skim milk for 1 hour. Plates were subsequently washed 8 times with PBS for the tween free protocol or 6 times with PBS-T and 2 times with PBS. 100μl TMB was the added to the wells and incubated for 30 minutes in the dark. HRP was then inactivated using 100 μl H_2SO_4 and absorbance was read at 450 nm. Absorbance was normalized, and EC50 was determined using GraphPad Prism's "nonlinear regression analysis for agonist binding" function.

2.1.9 Kinetics Assay and Kd calculation by Biacore Assay:

In order to gain a more accurate impression of antibody – target affinity as well as to determine on rate, off rate and a more precise Kd than the EC50 determined by ELISA a Biacore Assay was used, this consisted of 2 distinct stages.

Scouting of optimum receptor and antibody concentration ratios:

A range of concentrations of recombinant hFc - linked receptor was bound to a T200 Biacore chip on with 7000 RU anti-hFc had been immobilized previously. Samples of the recombinant receptor were suspended in PBS + 0.05% Tween20 and sequentially injected at a flow rate of 10 µl/min for 2 min at concentrations ranging from 0.78 µg/ml to 100 µg/ml. The concentration at which the anti-hFc binding reached saturation was determined. The concentration of hFc-recombinant receptor achieving anti-hFc binding saturation of the chip was used to for the kinetics assay. From this value, the concentration of BsAb yielding 100 RU when bound to the receptor was determined. This concentration along with 4 2 fold serial dilutions was used for the Kinetics assay. The chip was then regenerated using 3 M $MgCl_2$.

Biacore Kinetics Assay:

The recombinant receptor was bound to the chip at the concentration determined to yield saturation. Following binding of the recombinant hFc – linked receptor, BsAb was then injected at from the lowest to highest concentrations determined during scouting for 3 minutes at 10µl/min per concentration. And washed with PBS + 0.05% Tween20 at a flow rate of 30µl/min for 5 min.

2.1.10 Flow Cytometry Assays:

Flow cytometry analysis was employed to establish whether BsAb would bind to the native receptor found on the cell surface of selected tumour cell lines. Following confirmation of binding to the cell surface targets BsAb mediated colocalization of Cy5 labelled PEG nanoparticle and tumour cells were assayed.

Binding of BsAb to tumour cell surface targets:

Cells were grown to confluence in T80 static cell culture flasks, scraped and resuspended in 3.5 ml Advanced RPMI medium 1640 (Gibco) supplemented with 10% FCS and 1xGlutamax (Gibco). 100 µl of cells were then pelleted at 200 x g and washed in 100 µl 10% FCS-PBS. Cells were then re-pelleted and resuspended in 200 µg/ml antibody in PBSFCS. After 1 hour of incubation on ice, cells were again

pelleted and washed 3 times with 10% FCS-PBS. 50µl of 1/30 anti-c-myc-FITC in 10% FCS-PBS was then added to the cells and incubated for 1hr. Cells were washed 3 times with 10% FCS-PBS and resuspended in 100 µl 10% FCS PBS. Cells were then analysed using a BD LSR II Analyser until 20000 reads were accumulated. Data was analysed and graphed using Flowing 2.1 software (Flowingsoftware).

BsAb mediated colocalization of Cy5 labelled PEG nanoparticle and tumour cells

Each antibody (200 µg/ml) was preincubated with 0.10µg/ml Cy5 labelled nanoparticle (provided by Adrian Fuchs/Kris Thurecht) in 10% FCS-PBS for 30 min in the dark. MDA MB 468 cells were grown to confluence in T80 static cell culture flasks, scraped and resuspended in 3.5ml Advanced RPMI medium 1640 (Gibco). 100 µl of cells were then pelleted at 200 x g and washed in 100µl 10% FCS-PBS. Cells were then re-pelleted and resuspended in the antibody nanoparticle premix. After 1 hour of incubation on ice, cells were again pelleted and washed 3 times with 10% FCS-PBS. 50µl of 1/30 anti-c-myc-FITC in 10% FCS-PBS was then added to the cells and incubated for 1hr. Cells were washed 3 times with 10% FCS-PBS and resuspended in 100 µl 10% FCS PBS. Cells were then analysed using a BD LSR II Analyser until 20000 reads were accumulated. Data was analysed and graphed using Flowing 2.1

2.1.11 In Vivo Imaging:

Following the promising results of our flow cytometry study, we then went on to examine the performance of our BsAb in a xenograft mouse model. All animal studies were in accordance with guidelines of the Animal Ethics Committee of The University of Queensland (UQ), and Australian Code for the Care and Use of Animals for Scientific Purposes. Studies were undertaken to quantify the targeting efficiency of the BsAb Cy5 labelled nanoparticle complex in vivo. Nu/nu mice were implanted with MDA MB 468 on the flanks. Each mouse was injected subcutaneously with 2×10^6 MDAMB 468 cells. The imaging experiments were performed 8 days after tumour cell injections. Cy5 labelled nanoparticle (Control nanoparticle) and Cy5 labelled nanoparticle + anti-EGFR anti-15-2 BsAb (Targeted nanoparticle) were diluted in PBS to 20 mg/ml. 100 µl of Control and Targeted nanoparticle were injected via the tail vein into Mouse 1 and 2, respectively. Fluorescence and Xray images were acquired using an In-Vivo MS FX Pro imaging station. Mice were anaesthetized with 2% isoflurane during all procedures. Fluorescence readings of live mice were taken at 24, 48 and 96 hrs

2.1.12 Ex Vivo Imaging

Following Cy5 *in vivo* imaging at 96 hours, mice were euthanized, dissected and fluorescence of individual organs was assayed at 660nm using an In Vivo Ms FX Pro imaging station.

Chapter 3: Results and Discussion

3.1 Development and design of anti-PEG anti-EGFR Bispecific Antibodies:

Our initial efforts focussed on finding the best binding partner for our PEG nanoparticle; to achieve this we designed a total of 5 BsAbs (Appendix A: Figure 2) each consisting of an anti-EGFR scFv and a distinct anti-PEG scFv. The EGFR scFv has previously been described in detail and has been shown to bind EGFR with a K_D of 5.2 $x10^{-10}$M (Taylor et al 2015).

3.1.1 Construct 1; anti-EGFR- PEG (Panitumumab-15-2):

The monoclonal antibody 15-2 is a type IgG2b antibody that can detect unmodified as well as methoxyl-PEG in an ELISA setting to concentrations at the nanogram level (Chen et al. 2012). Upon reformatting into BsAb format and insertion into the NBF347 plasmid, the anti-EGFR-PEG(15-2) construct expressed well in a CHO transient expression system and yielded ~28mg/L of cell culture. The SDS-PAGE analysis indicated that the BsAb can be purified to high purity as it binds to both Hi-Trap and Protein L columns (Appendix A: Figure 4). Whilst purification via the HIS-tag with a Hi-Trap column yielded a comparatively impure product, purification with a Protein L column yielded BsAb of high purity.

Analysis with SEHPLC indicated the presence of both monomeric BsAb as well as higher order aggregates at approximately equal proportions (Appendix A: Figure 8 (Panel B)). The presence of aggregate is likely a result of oxidation of free cysteine residues in the monomer. BsAb purifications appeared to contain no significant impurities.

DLS assays showed the presence of some antibody aggregate (Appendix A: Figure 9 (Panel B)). Data indicates that 72% of BsAb is present as a monomer with a spherical size of 7.42 nm.

Affinity screening using ELISA showed the BsAb to bind to both EGFR as well as the methoxyl-PEG nanoparticle, but not LPS at a concentration of 100 μg/ml (Appendix A: Figure 10). The BsAb displays a high affinity estimated to be 491 pM +- 71 pM (Appendix A: Figure 18) to immobilized methoxyl-PEG nanoparticles. The anti-EGFR-LPS control displayed no dose-dependent binding (Appendix A: Figure 19). PEG binding disruption by Tween20 may be influenced by the cell surface target scFv linked to anti-

PEG scFv and/or may be a result of the structural similarity of PEG and Tween20 (Appendix A: Figure 24). Analysis of further antibody flow cytometry assays showed that the BsAb binds to MDA MB 468 cells *in vitro* (Appendix A: Figure 28). MDA MB 468 has previously been shown to overexpress EGFR. The BsAb induces co-localization of Cy5 labelled PEG nanoparticles to MDA MB 468 cells *in vitro* (Appendix A: Figure 30).

Imaging of Cy5 labelled nanoparticle co injected with our BsAb showed a degree of BsAb mediated co-localization of nanoparticle and MDA MB 468 xenograoft cells *in vivo* using MDA MB 468 xenografts in nu/nu mice (Appendix A: Figure 31). At 24 and 48 hours, tumours of mice injected with the BsAb-bound nanoparticle showed significantly higher fluorescence than tumours of mice injected only with the nanoparticle. Furthermore, this BsAb increased amounts of the nanoparticle retained within the tumour mass even at 96 hours. Nanoparticle retained in the tumour of the mouse treated with untargeted nanoparticle likely has accumulated there as a result of EPR.

Cy5 fluorescence imaging of organs *ex vivo*, extracted at 96 hours (Appendix A: Figure 32) showed the nanoparticle to be fully cleared from blood when injected as a mixture of this BsAb and nanoparticle. However, there were also a significant presence of nanoparticle within the tissues of the liver and spleen. This is likely a result of the aggregate present in the initial BsAb purification and will need to be investigated and optimized further.

3.1.2 Construct 2; anti-EGFR-PEG (Panitumumab-AGP3):

The monoclonal antibody AGP3 is a type IgM antibody that can detect both unmodified as well as methoxyl-PEG in an ELISA setting to concentrations at the nanogram level (Chen et al. 2012). Upon reformatting into BsAb format and insertion into the NBF347 plasmid, the anti-EGFR-PEG(AGP3) construct expressed well in a CHO transient expression system and yielded ~15.5mg/L of cell culture. Following purification the BsAb bound EGFR but there was no binding to methoxyl-PEG nanoparticle or LPS at a concentration of 100μg/ml (Appendix A: Figure 11), and no dose-response relationship between methoxyl-PEG nanoparticle binding and BsAb concentration could be established (Appendix A: Figure 20) and further investigation of this BsAb was thus abandoned in favour of the 15-2 derived scFv.

3.1.3 Construct 3; anti-EGFR-PEG (Panitumumab-3.3):

The monoclonal antibodies 3.3 is a type IgG1 antibody that can detect unmodified PEG in an ELISA setting, but there is no information as to the antibody's affinity (Chen et al. 2012).). Upon reformatting into BsAb format and insertion into the NBF347 plasmid, the anti-EGFR-PEG(3.3) construct expressed in a CHO transient expression system and yielded ~12mg/L of cell culture. Following purification the BsAb bound EGFR but there was no binding to methoxyl-PEG nanoparticle or LPS at a concentration of 100μg/ml (Appendix A: Figure 12), further investigation of the 3.3 derived scFv was thus abandoned in favour of the 15-2 derived scFv.

3.1.4 Construct 4; anti-EGFR-PEG (Panitumumab-6.3):

The monoclonal antibody 6.3 is a type IgG1 antibody that can detect unmodified PEG in an ELISA setting, but there is no information as to the antibody's affinity (Chen et al. 2012). Upon reformatting into BsAb format and insertion into the NBF347 plasmid, the anti-EGFR-PEG(6.3) construct expressed poorly in a CHO transient expression system and yielded ~1.3mg/L of cell culture. Following purification the BsAb bound EGFR but there was no binding to the methoxyl-PEG nanoparticle or LPS at a concentration of 100μg/ml (Appendix A: Figure 13), further investigation of the 6.3 derived scFv was thus abandoned in favour of the 15-2 derived scFv.

3.1.5 Construct 5; anti-EGFR-PEG (Panitumumab-E11):

The monoclonal antibody E11 is a type IgG1 antibody that can detect unmodified PEG in an ELISA setting, but there is no information as to the antibody's affinity (Chen et al. 2012). Upon reformatting into BsAb format and insertion into the NBF347 plasmid, the anti-EGFR-PEG(E11) construct expressed well in a CHO transient expression system and yielded ~12.5mg/L of cell culture. Following purification the BsAb did not bind EGFR nor was there binding to the methoxyl-PEG nanoparticle or LPS at a concentration of 100μg/ml (Appendix A: Figure 14) and further investigation of the E11 derived scFv was thus abandoned in favour of the 15-2 derived scFv.

3.2 Development of BsAbs targeting novel cancer cell surface targets

After demonstration of efficacious binding to, as well as co-localization, of targeted methoxyl-PEG nanoparticles to MDA MB 468 with anti-EGFR-PEG(15-2) BsAb both *in vitro* and *in vivo* utilizing both

flow cytometry and fluorescence *in vivo* imaging, three further BsAbs were designed, using the 15-2 anti-PEG scFv, to target novel potential cancer cell surface markers. This work is to further validate the BsAb targeted PEG nanoparticle towards targets other than EGFR.

3.2.1 Construct 6; anti-CD171-PEG (L1_9.3Hu – 15-2):

The anti-CD171 scFv was designed from variable regions identified from the humanized monoclonal antibody published by Kelm et al. (2012). CD171, or L1-CAM, was chosen as a cell surface target of interest, as there is evidence that CD171 is present in a large proportion of chemotherapy-resistant cancers. CD171 traditionally is associated with both cell adhesion and motility of neural cells. Cancers expressing CD171 have been associated with poor patient survival. Expression of CD171 has been associated with a drop as high as 70% in 5-year survival prognosis in colorectal cancer (Fang et al. 2010). CD171 is not present outside of the central nervous system in adults and as such has potential applications as a targeting antibody for cancer therapeutics.

Upon reformatting into the BsAb format and insertion into the NBF347 plasmid, we found that the anti-CD171-PEG construct expressed well in a CHO transient system and yield of ~36mg/L of cell culture. The BsAb and can be purified to high purity as it binds to both Hi-Trap and Protein L columns (Appendix A: Figure 5). Whilst purification via the HIS-tag with a Hi-Trap column yields a comparatively impure product, purification with a Protein L column yields BsAb of high purity.

Analysis with SEHPLC indicated the presence of both monomeric as well as dimeric and quatrimeric BsAb but no higher order aggregates (Appendix A: Figure 8 (Panel C)). BsAb purifications appeared to contain no significant impurities.

DLS showed the presence of no antibody aggregate (Appendix A: Figure 9 (Panel C)). Data indicates that antibody is present at an average spherical size of 8.09 nm. Furthermore addition of PEG-Nanoparticle to anti-Cd171-PEG BsAb correlated in a dose-dependent manner with an increase in average particle size, anti-Cd171-PEG BsAb shows and average size of 10.1nm, anti-Cd171-PEG BsAb + 1 μg Nanoparticle shows and average size of 11.7 nm, anti-Cd171-PEG BsAb + 10 μg Nanoparticle shows and average size of 15.7, anti-Cd171-PEG BsAb + 100 μg nanoparticle shows and average size of 11.3 & 43.8 whilst 100 μg Nanoparticle shows and average size of 5.9 nm (Appendix A: Figure 25). This is indicative of binding of nanoparticle and BsAb.

Affinity screening using ELISA showed the BsAb to exhibit high affinity to CD171 as well as the methoxyl-PEG nanoparticle but not CD200, CD 223 or EGFR at a concentration of 100 μg/ml, binding to the methoxyl-PEG nanoparticle is undisrupted by Tween 20 (Appendix A: Figure 15). This strengthens our prior assumption that the non-PEG scFv may have an impact on the affinity of the anti-PEG scFv. The BsAb displayed high affinity, estimated to be 15+-4pM, to immobilized CD171 (Appendix A: Figure 21).

The affinity of the anti-Cd171-PEG BsAb was further assessed by Biacore. During scouting of optimal assay conditions L1 cell adhesion molecule/hFc recombinant (150 kDa) reached saturation on chip 42 fc3 4 (7000RU anti-hFc immobilised previously) with 1764RU at a concentration of 100 μg/ml in running buffer, subsequent application of 200μg/ml of anti-Cd171-PEG BsAb in running buffer yielded a response of approximately 100RU.

From the Scouting, we determined optimum conditions to constitute of an initial immobilization of 50μg/ml L1 cell adhesion molecule/hFc recombinant to achieve a receptor saturation of 1100RU followed by the application of 5 BsAb concentrations, 200.30 nM, 400.60 nM, 900.21 nM, 1.84 uM, and 3.68 uM. These yielded responses of 6 RU, 19 RU, 39 RU, 89 RU and 118 RU respectively (Appendix A: Figure 26). Analysis with Biacore control software (v2.0) using an assumed 1:1 binding ratio of anti-Cd171-PEG BsAb to L1 cell adhesion molecule/hFc recombinant yielded in a calculated K_D of $3.45E^{-07}$ with a k_a of $2.30E^{+04}$ and a k_d of $7.94E^{-3}$. This is approximately 1000 fold less than the expected KD indicated by the ELISA assay. However, this KD still falls within the expected range of affinities of scFv based antibody constructs.

Flow cytometry assays showed that the anti-CD171-PEG BsAb will bind to SKOV-3 (Appendix A: Figure 29) but not MDA MB 468 (Appendix A: Figure 28) cells *in vitro*.

3.2.2 Construct 7; anti-CD200-PEG (Samalizumab – 15-2):

The anti-CD200 scFv was designed from variable regions identified from the humanized monoclonal antibody published by Bowdish et al. (2004). CD200 or OX-2 is associated with the stem cell-like characteristics of cells that are thought to be present in dormant cancer stem cells, which may be present at the hypoxic centre of tumours. It has also been shown to be a potent tumour response suppressor. CD200 overexpression has been correlated with an increased probability of relapse following

chemotherapy, and a more aggressive disease phenotype than observed in non or low expressing tumours; this furthers the hypothesis of CD200 as a cancer stem cell marker.

Upon reformatting into BsAb format and insertion into the NBF347 plasmid, we found that the anti-CD200-PEG construct expressed well in a CHO transient system and yield of 12.8 mg/L of cell culture. The BsAb and can be purified to high purity as it binds to both Hi-Trap and Protein L columns (Appendix A: Figure 6). Whilst purification via the HIS-tag with a Hi-Trap column yields a comparatively impure product, purification with a Protein L column yields BsAb of high purity.

Analysis with SEHPLC indicated the presence of both monomeric as well as dimeric and quatrimeric BsAb as well as higher order aggregates (Appendix A: Figure 9 (Panel D)). BsAb purifications appear to contain no significant impurities.

DLS showed the presence of some antibody aggregate (Appendix A: Figure 9 (Panel D)). Data indicates that antibody is present principally as a multimer at an average spherical size of 15.88 nm.

Affinity screening using ELISA showed the BsAb to exhibit high affinity to CD200 as well as the methoxyl-PEG nanoparticle but not CD171, CD 223 or EGFR at a concentration of 100μg/ml, binding to the methoxyl-PEG nanoparticle is disrupted by Tween 20 (Appendix A: Figure 16). The BsAb displayed high affinity estimated to be 38+-8 pM to immobilized CD200 (Appendix A: Figure 22) and binds immobilized nanoparticle.

The affinity of the anti-Cd171-PEG BsAb was further assessed by Biacore. During scouting of optimal assay conditions RhCD200/hFc recombinant receptor (49kDa) reached saturation on chip 42 fc3 4 (7000RU anti-hFc immobilised previously) with 280 RU at a concentration of 1.5625 μg/ml in running buffer, subsequent application of 12.5 μg/ml of anti-CD200-PEG BsAb in running buffer yielded a response of approximately 194 RU.

From the Scouting, we determined optimum conditions to constitute of an initial immobilization of 0.78125μg/ml RhCD200/hFc recombinant receptor to achieve a receptor saturation of 150 RU followed by the application of 5 BsAb concentrations, 7.18 nM, 10.44nM, 20.87nM, 50.76nM and 100.15nM. These yielded responses of 14RU, 36RU, 70RU, 91RU and 104RU respectively (Appendix A: Figure 27). Analysis with Biacore control software (v2.0) using an assumed 1:1 binding ratio of anti-CD200-PEG BsAb to RhCD200/hFc recombinant receptor yielded in a calculated K_D of $1.20E^{-08}$ with a k_a of

$4.32E^{08}$ and a k_d of 5.20. This is approximately 1000 fold less than the expected KD indicated by the ELISA assay. This KD still falls within the expected range of affinities of scFv based antibody constructs.

3.2.3 Construct 8; anti-CD227-PEG (clivatuzumab tetraxetan – 15-2):

The anti-CD227 scFv was designed from variable regions identified from the humanized monoclonal antibody with affinity to the PAM4 epitope of CD227 published by Gold et al. (2003). CD227 or MUC-1 is thought to be one of the mucins responsible for chemotherapeutic resistance by forming a mucinous cocoon around a tumour, thus inhibiting access of immune cells and chemotherapeutics to the tumour, as well as retaining growth factors secreted by tumour associated cells. However, MUC-1 is a membrane-associated protein and as such should be subject to membrane turnover allowing for internalization of mucin bound protein. Furthermore, MUC-1 has been shown to interact with both p53 and Bcl-2-Associated death promoter to inhibit apoptosis.

Upon reformatting into BsAb format and insertion into the NBF347 plasmid, we found that the anti-CD227-PEG construct expressed more poorly than the other tandem BsAbs in a CHO transient system and yielded of ~8.75mg/L of cell culture. The BsAb and can be purified to high purity as it binds to both Hi-Trap and Protein L columns (Appendix A: Figure 7). Whilst purification via the HIS-tag with a Hi-Trap column yields a comparatively impure product, purification with a Protein L column yields BsAb of high purity.

Analysis with SEHPLC indicateed the presence of no monomeric or dimeric and only small quantities of quatrimeric BsAb as well as a high proportion higher order aggregates (Appendix A: Figure 8 (Panel E)). BsAb purifications appear to contain no significant impurities.

DLS showed the presence of large amounts of antibody aggregate (Appendix A: Figure 9 (Panel E)). Data indicates that no antibody monomer is present.

Affinity screening using ELISA showed the BsAb to exhibit an affinity to the methoxyl-PEG nanoparticle but not CD171, CD200, CD 223 or EGFR at a concentration of 100μg/ml, binding to the methoxyl-PEG nanoparticle is disrupted by Tween 20 (Appendix A: Figure 17). The BsAb displays some affinity estimated to be ~60nM to immobilized CD223 (Appendix A: Figure 23).

4 Conclusion

Our work shows that anti-EGFR-PEG BsAb can be used to target methoxyl-PEG nanoparticle to immobilized recombinant EGFR *in vitro* as well as native EGFR on MDA MB468 cells *in vitro* and *in vivo*. This shows great promise as a means of targeting EGFR overexpressing tumours with PEGylated drugs. Furthermore, we have shown that it is possible to construct further functional BsAbs from published sequences of monoclonal antibodies. We have shown that anti-Cd171-PEG BsAb can be used to target both immobilized Cd171 as well as SKOV-3 cells in vitro. We also show that anti-Cd200-PEG BsAb will bind to immobilized Cd200 *in vitro*. Further work should focus on the validation of the anti-Cd200-PEG BsAb *in vitro* and *in vivo* xenograft imaging with both anti-Cd171-PEG and anti-Cd200-PEG BsAb. Furthermore the relationship of target ScFv backbone sequence and BsAb stability in arginine buffer should be investigated further.

5 Research Environment

Infrastructure for this project was provided by the Mahler/Gray group, who also has access to the protein expression facilities of the National Biologics Facility (NBF) located at AIBN. NBF has extensive knowledge regarding the engineering of scFv antibodies, and mammalian protein expression and purification, which will assist in the fulfilment of the project aims. *In vitro* assays were conducted at Queensland Brain Institute's (QBI) FACS lab.

The Thurecht group has provided PEG nanoparticles and also has access to extensive imaging facilities at ACMRI, which have been put at the disposal of Mahler group in collaboration with this project.

6 Role of Personnel

A/Prof Mahler has experience and expertise in protein engineering and antibody design, whilst Dr. Howard is an expert in mammalian BsAb expression and in vitro imaging. Dr. Thurecht is an expert on the design, production, and characteristics of PEG nanoparticles, as well as in vivo imaging of xenograft mice. Geoff Osborne of QBI's Flow Cytometry Facility has been of invaluable assistance in conducting my flow cytometry protocols. To date, my advisory team has been able to provide me with all advice and insight into the development of BsAbs required. Furthermore, personnel from Gray/Mahler group have been able to provide me with advice on developing the required methodologies, familiarizing myself with new instruments and achieving experimental goals required for this project.

7 References

Arruebo M, Valladares M, Gonzales-Fernandez A. Antibody-Conjugated Nanoparticles for Biomedical Applications. Journal for nanomaterials. Vol 2009. Article ID: 439389 doi:10.1155/2009/439389

Bowdish KS, McWhiter J, Kretz-Rommel A, Maruyama T. Polypeptides and antibodies derived from chronic lymphotic leukemia cells and uses thereof. United States Patent Publication Nov. 23, 2004 US7408041 B2

Brischwein K, Schlereth B, Guller B, Steiger C, Wolf A, Lutterbuese R, Offner S, Locher M, Urbig T, Raum T, Kleindienst P, Wimberger P, Kimmig R, Fichtner I, Kufer P, Hofmeister R, da Silva AJ, Baeuerle PA. MT110: a novel bispecific single-chain antibody construct with high efficacy in eradicating established tumors. Mol Immunol. 2006 Mar;43(8):1129-43.

Burden RE, Caswell J, Fay F, Scott CJ. Recent advances in the application of antibodies as therapeutics. Future Medicinal Chemistry. 2012. 4(1):73-86

Chen T, Roffler S, Chuang K, Lu S. Anit-Polyethylene Glycol Antibody Expressing Cell Quantify and Free Polyethylene Glycol and Polyethylene Glycol-Derivatized Molecules. Unites States Patent Application Publication. Jan. 19, 2012. US20120015380 A1

Coles DJ, Rolfe BE, Boase NR, Veedu RN, Thurecht KJ. Aptamer-targeted hyperbranched polymers: towards greater specificity for tumours in vivo. Chem Commun (Camb). 2013 May 10;49(37):3836-8. doi: 10.1039/c3cc00127j.

Ellerman D, Scheer JM. Generation of Bispecific Antibodies by Chemical Conjugation. New York: Springer, 2011 47-63

Fang Q, Lu L, Yang B, Zhao Z, Wu Y, Zheng X. L1, B-Ctenin and E-Cadherin Expression in Patients with Colorectal Cancer: Correlation with Clinicopathologic Features and it's prognostic significance. Journal of Surgical Oncology 2010; 102:433-442

Ferlay J, Soerjomataram I, Ervik M, Dikshit R, Eser S, Mathers C, Rebelo M, Parkin DM, Forman D, Bray, F (2013). GLOBOCAN 2012 v1.0, Cancer Incidence and Mortality Worldwide:IARC CancerBase No. 11 [Internet]. Lyon, France:International Agency for Research on Cancer.

Firer MA. Antibody-drug conjugates in cancer therapy filling in the potholes that lie ahead. OA Cancer 2013 Jun 19;1(1):8.

Gerber DE. Targeted therapies: a new generation of cancer treatments. Am Fam Physician. 2008 Feb 1;77(3):311-9.

Gold DV, Goldenberger DM, Hansen H. Monoclonal antibody PAM4 and its use for diagnosis and therapy of pancreatic cancer. European Union Patent Application. Jun. 16, 2003. EP1521775 (A1)

Goodall S, Jones ML, Mahler S. Monoclonal antibody-targeted polymeric nanoparticles for cancer therapy – future prospects. J. Chem. Technol. Biotechnol. 2014. Sep 1097-4660 doi: 10.1002/jctb.4555

Holliger P, Hudson PJ. Engineered antibody fragments and the rise of single domains. Nat Biotechnol. 2005 Sep;23(9):1126-36.

Howard CB, Fletcher N, Houston ZH, Fuchs AV, Boase NR, Simpson JD, Raftery LJ, Ruder T, Jones ML, de Bakker CJ, Mahler SM. Overcoming Instability of Antibody-Nanomaterial Conjugates: Next Generation Targeted Nanomedicines Using Bispecific Antibodies. Adv Healthc Mater. 2016 Aug;5(16):2055-68. doi: 10.1002/adhm.201600263. Epub 2016 Jun 10.

Pan H, Soman NR, Schlesinger PH, Lanza GM, Wickline SA. Cytolytic peptide nanoparticles ('NanoBees') for cancer therapy. Wiley Interdiscip Rev Nanomed Nanobiotechnol. 2011 May-Jun;3(3):318-27. doi: 10.1002/wnan.126.

Jakobovits A, Yang X, Gallo M, Jia X. Human monoclonal antibodies to epidermal growth factor receptor. Unites States Patent Application Publication. May 22 2001. US6235883 B1

Joensson F, Mancardi DA, Zhao W, Kita Y, Iannascoli B, Khun H, Van Rooijen N, Shimizu T, Schwartz LB, Daeron M, Bruhns P. Human FcγRIIA induces anaphylactic and allergic reactions. Blood. 2012 Mar 15;119(11);DOI 10.1182.

Kelm A, Altevogt P, Moldenhauer G, Brietling F, Krueger A, Baerreiter S, Luettgau S, Moebius U. Treatment of tumors using specific Anti-L1 Antiody. United States Patent Application Publication. Mar. 20, 2012. US8138313B2

Langer M, Kratz F, Rothen-Rutishauser B, Wunderli-Allenspach H, Beck-Sickinger AG. Novel peptide conjugates for tumor-specific chemotherapy. J Med Chem. 2001 Apr 26;44(9):1341-8.

Meisel K and Rizvi SA. Complications of Monoclonal Antibody Therapy. Medicine & Health. 2011 Nov; 94(11)

Oettle H, Post S, Neuhaus P, Gellert K, Langrehr J, Ridwelski K, Schramm H, Fahlke J, Zuelke C, Burkart C, Gutberlet K, Kettner E, Schmalenberg H, Weigang-Koehler K, Bechstein WO, Niedergethmann M, Schmidt-Wolf I, Roll L, Doerken B, Riess H. Adjuvant chemotherapy with gemcitabine vs observation in patients undergoing curative-intent resection of pancreatic cancer: a randomized controlled trial. JAMA. 2007 Jan 17;297(3):267-77.

Roland E Kontermann. Dual targeting strategies with bispecific antibodies. MAbs. 2012 Mar-Apr; 4(2): 182–197. Published online 2012 Mar 1. doi: 10.4161/mabs.4.2.19000

Sanna V, Pala N, Sechi M. Targeted therapy using nanotechnology: focus on cancer. Int J Nanomedicine. 2014 Jan 15;9:467-83. doi: 10.2147/IJN.S36654. eCollection 2014.

Spiess C, Zhai Q, Carter P J. Alternative molecular formats and therapeutic applications for bispecific antibodies. Mol Immunol., 2015 Oct ; 67(2): 95-106. Doi: 10. 1016/j.molimm.2015.01.003

Taylor K, Howard CB, Jones ML, Sedliarou I, MaCDiarmid J, Brahmbhatt H, Munro TP, Mahler SM. Nanocell targeting using engineered bispecific antibodies. MAbs. 2015 Jan 2;7(1):53-65. doi: 10.4161/19420862.2014.985952.

Von Minckwitz G, Harder S, Hövelmann S, Jäger E, Al-Batran S, Loibl S, Atmaca A, Cimpoiasu C, Neumann A, Abera A, Knuth A, KaufmannM, Jäger D, Maurer AB, Wels WS. Phase I clinical study of the recombinant antibody toxin scFv(FRP5)-ETA specific for the ErbB2/HER2 receptor in patients with advanced solid malignomas. Breast Cancer Research. 2005 Jun 1. 7(5):R617-26

Wang Z, Liu G, Zheng H, Chen X. Rigid nanoparticle-based delivery of anti-cancer siRNA: challenges and opportunities. Biotechnol Adv. 2014 Jul-Aug;32(4):831-43. doi: 10.1016/j.biotechadv.2013.08.020.

Yoo J-W, Irvine DJ, Discher DE Mitragotri Bio-inspired, bioengineered and biomimetic drug delivery carriers. Nature Reviews Drug Discovery. 2011. 10(7):521-535.

8 Appendix A – Figures

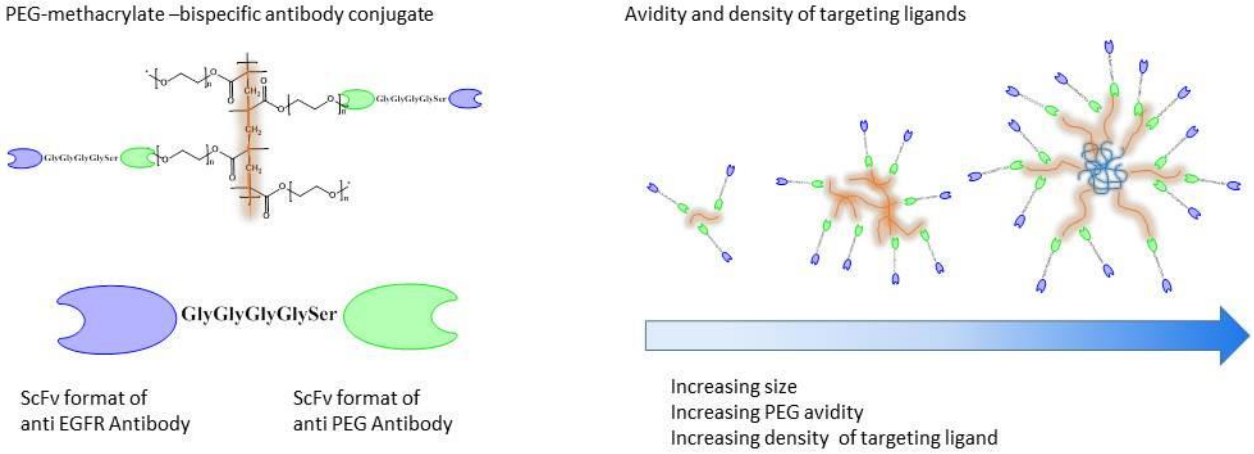

Figure 1: Illustration of the relationship between nanoparticle size and targeting ligand density. (Figure adapted from Howard et al.)

>Vect_G4S_Peg15-2 (anti-EGFR-PEG(15-2)BsAb)

HindIII site-
MGWSCIILFLVATATGVHSHHHHHHQLQLQESGPGLVKPSETLSLTCTVSGGSVSSGDYYWTWIRQSPGKGLEWIGHIYYSGNTNYNPSLKS
RLTISIDTSKTQFSLKLSSVTAADTAIYYCVRDRVTGAFDIWGQGTMVTVSSGGGGSGGGGSGGGGSDIQMTQSPSSLSASVGDRVTITCQA
SQDISNYLNWYQQKPGKAPKLLIYDASNLETGVPSRFSGSGSGTDFTFTISSLQPEDIATYFCQHFDHLPLAFGGGTKVEIKSGGGGSEVKL
EESGGGLVQPGGSMKLSCVASGFTFSNYWMNWVRQSPEKGLEWVTEIRSKSNNYATHYAESVKGRFTISRDDSKGSVYLQMNNLRAEDTGIY
YCSNRYYWGQGTLVTVSAGGGGSGGGGSGGGGSDIVMTQSHKFMSTSVRDRVTITCKASQDVNTSVAWYQQKPGQSPKLVIYWASTRHTGVP
DRFTGSGSGTDFTLTISNVQSEDLADYFCLQYINYPYTFGGGTKLEIKEQKLISEEDLN* - NotI site

>Vect G4S PEGAGP3 (anti-EGFR-PEG(AGP3)BsAb)
HindIII site-
MGWSCIILFLVATATGVHSHHHHHHQLQLQESGPGLVKPSETLSLTCTVSGGSVSSGDYYWTWIRQSPGKGLEWIGHIYYSGNTNYNPSLKS
RLTISIDTSKTQFSLKLSSVTAADTAIYYCVRDRVTGAFDIWGQGTMVTVSSGGGGSGGGGSGGGGSDIQMTQSPSSLSASVGDRVTITCQA
SQDISNYLNWYQQKPGKAPKLLIYDASNLETGVPSRFSGSGSGTDFTFTISSLQPEDIATYFCQHFDHLPLAFGGGTKVEIKSGGGGSEVQL
VESGGGLVKPGGSLKLSCAASGFTFSDYYMYWVRQTPEKRLEWVATISDDGTYTYYPHSVKGRFTISRDSAKNNLYLQLSSLKSEDTAMYYC
ARNDARGDYWGQGTSVTVSSGGGGSGGGGSGGGGSDIVLTQAAFSNPVTLGTSASISCRSSKSLLHSNGITYLYWYLQKPGQSPQLLIYQMS
NLASGVPDRFSSSGSGTDFTLRISRVEAEDVGVYYCAQNLELFTFGSGTKLEIKEQKLISEEDLN* - NotI site

>Vect_G4S_PEG3-3 (anti-EGFR-PEG(3-3)BsAb)
HindIII site-
MGWSCIILFLVATATGVHSHHHHHHQLQLQESGPGLVKPSETLSLTCTVSGGSVSSGDYYWTWIRQSPGKGLEWIGHIYYSGNTNYNPSLKS
RLTISIDTSKTQFSLKLSSVTAADTAIYYCVRDRVTGAFDIWGQGTMVTVSSGGGGSGGGGSGGGGSDIQMTQSPSSLSASVGDRVTITCQA
SQDISNYLNWYQQKPGKAPKLLIYDASNLETGVPSRFSGSGSGTDFTFTISSLQPEDIATYFCQHFDHLPLAFGGGTKVEIKSGGGGSEVKL
EESGGGLVQPGGSMKLSCAASGFIFSDAWMDWVRQSPERGLEWVAEIRSKANGLAPYYAESVKGRFTISRDDSKSSVYLQMNNLRSEDTGIY
YCTSTLYYFDYWGQGTTLTVSSGGGGSGGGGSGGGGSQIVLTQSPAIMSAFPGERVTLTCSASSSVRSSYLCWYQQKPGSSPKLWIYSTSNL
ASGVPARFSGSGSGTSYSLTISSMEAEDAASYFCHQWSSYPRTFGGGTKLEIKEQKLISEEDLN* - NotI site

>Vect_G4S_PEG6-3 (anti-EGFR-PEG(6-3)BsAb)
HindIII site-
MGWSCIILFLVATATGVHSHHHHHHQLQLQESGPGLVKPSETLSLTCTVSGGSVSSGDYYWTWIRQSPGKGLEWIGHIYYSGNTNYNPSLKS
RLTISIDTSKTQFSLKLSSVTAADTAIYYCVRDRVTGAFDIWGQGTMVTVSSGGGGSGGGGSGGGGSDIQMTQSPSSLSASVGDRVTITCQA
SQDISNYLNWYQQKPGKAPKLLIYDASNLETGVPSRFSGSGSGTDFTFTISSLQPEDIATYFCQHFDHLPLAFGGGTKVEIKSGGGGSQIQL
VQSGPELKKPGETVKISCKASGYTFKNYGMNWVKQAPGKGLKWMGWINTYTGQPIYANDFKGRFAFSLETSASTAYLQINNLKNEDTATYFC
ARDWGPYWGQGTLVIVSAGGGGSGGGGSGGGGSNIMMTQSPSSLAVSAGEKVTVNCKSSQSVLYSSNQMNYLAWYQQKPGQSPKLLIYWAST
RESGVPDRFTGSGSGTDFTLTISSVQTEDLAVYYCLQYLSSWTFGGGTKLEIKEQKLISEEDLN* - NotI site

>Vect G4S PEGE11 (anti-EGFR-PEG(E11)BsAb)
HindIII site-
MGWSCIILFLVATATGVHSHHHHHHQLQLQESGPGLVKPSETLSLTCTVSGGSVSSGDYYWTWIRQSPGKGLEWIGHIYYSGNTNYNPSLKS
RLTISIDTSKTQFSLKLSSVTAADTAIYYCVRDRVTGAFDIWGQGTMVTVSSGGGGSGGGGSGGGGSDIQMTQSPSSLSASVGDRVTITCQA
SQDISNYLNWYQQKPGKAPKLLIYDASNLETGVPSRFSGSGSGTDFTFTISSLQPEDIATYFCQHFDHLPLAFGGGTKVEIKSGGGGSQVQL
QESGAELARPGASVMMSCKASGYTFTTYTMNWVKQRPGQGLEWIGYIIPSSGYVDYNQKFKGKTILTTDKSSSTAYMQLSSLTSEDSAVYYC
VRSLDGYFWFAYWGQGTVVTVSAGGGGSGGGGSGGGGSDVLMTQSPLSLPVSLGDHASISCRSSKSIVHSNGNTYLEWFLQKPGQSPKLLIY
KVSKRMSGVPDRFSGSGSGTDFTLKIRRVEAEDLGVYYCSQGSHVPPTFGGGTKLEIKEQKLISEEDLN* - NotI site

>L19.3Hu_G4S_Peg15-2 (anti-CD171-PEG(15-2)BsAb)
HindIII site-
MGWSCIILFLVATATGVHSHHHHHHEVQLVQSGGGLVQSGGSLRLSCEQSGEEFERYWMLWVRQRPGHGLEWVGEINPRNDRTNY
NEKFKTRFTISVDRSKSTAYLQMDSLRAEDTAVYFCALGGGYAMDYWGQGTLVTVSSGGGGSGGGGSGGGGSDIQMTQSPSSL
SASVGDRVTITCRASQDISNYLNWYQQKPGKAPKLLIYYTSRLHSGVPSRFSGSGSGTDYTLTISSLQPEDFATYFCQQGNTL
PWTFGGGTKLEIKRSGGGGSEVKLEESGGGLVQPGGSMKLSCVASGFTFSNYWMNWVRQSPEKGLEWVTEIRSKSNNYATHYAESVKGRF
TISRDDSKGSVYLQMNNLRAEDTGIYYCSNRYYWGQGTLVTVSAGGGGSGGGGSGGGGSDIVMTQSHKFMSTSVRDRVTITCKASQDVNTSV
AWYQQKPGQSPKLVIYWASTRHTGVPDRFTGSGSGTDFTLTISNVQSEDLADYFCLQYINYPYTFGGGTKLEIKEQKLISEEDLN* -
NotI site

>CD200_G4S_Peg15-2 (anti-CD200-PEG(15-2)BsAb)
HindIII site-
MGWSCIILFLVATATGVHSHHHHHHQVQLQQSGSELKKPGASVKISCKASGYSFTDYIILWVRQNPGKGLEWIGHIDPYYGSSNYNLKFKGR
VTITADQSTTTAYMELSSLRSEDTAVYYCGRSKRDYFDYWGQGTTLTVSSGGGGSGGGGSGGGGSDIQMTQSPSSLSASIGDRVTITCKASQ
DINSYLSWFQQKPGKAPKLLIYRANRLVDGVPSRFSGSGSGTDYTLTISSLQPEDFAVYYCLQYDEFPYTFGGGTKLEIKRSGGGGSEVKLE
ESGGGLVQPGGSMKLSCVASGFTFSNYWMNWVRQSPEKGLEWVTEIRSKSNNYATHYAESVKGRFTISRDDSKGSVYLQMNNLRAEDTGIYY
CSNRYYWGQGTLVTVSAGGGGSGGGGSGGGGSDIVMTQSHKFMSTSVRDRVTITCKASQDVNTSVAWYQQKPGQSPKLVIYWASTRHTGVPD
RFTGSGSGTDFTLTISNVQSEDLADYFCLQYINYPYTFGGGTKLEIKEQKLISEEDLN* - NotI site

>MUC1_G4S_Peg15-2 (anti-CD223-PEG(15-2)BsAb)
HindIII site-
MGWSCIILFLVATATGVHSHHHHHHQVQLQQSGAEVKKPGASVKVSCEASGYTFPSYVLHWVKQAPGQGLEWIGYINPYNDGTQYNEKFKGK
ATLTRDTSINTAYMELSRLRSDDTAVYYCARGFGGSYGFAYWGQGTLVTVSSGGGGSGGGGSGGGGSDIQLTQSPSSLSASVGDRVTMTCSA
SSSVSSSYLYWYQQKPGKAPKLWIYSTSNLASGVPARFSGSGSGTDFTLTISSLQPEDSASYFCHQWNRYPYTFGGGTRLEIKSGGGGSEVK
LEESGGGLVQPGGSMKLSCVASGFTFSNYWMNWVRQSPEKGLEWVTEIRSKSNNYATHYAESVKGRFTISRDDSKGSVYLQMNNLRAEDTGI
YYCSNRYYWGQGTLVTVSAGGGGSGGGGSGGGGSDIVMTQSHKFMSTSVRDRVTITCKASQDVNTSVAWYQQKPGQSPKLVIYWASTRHTGV
PDRFTGSGSGTDFTLTISNVQSEDLADYFCLQYINYPYTFGGGTKLEIKEQKLISEEDLN* - NotI site

Figure 2: FASTA format sequences of designed BsAbs.

Initial development of our BsAbs involved the identification of the variable heavy (yellow) and light domains (green) from sequences of monoclonal antibodies with affinity to EGFR, MUC1, OX-2 and L1CAM. The anti-PEG scFv sequences are shown in gray. The derived scFvs were then linked by a G4S linker. His and c-myc tags (cyan) were also added to bispecific antibody to allow for easy purification and detection in assays.

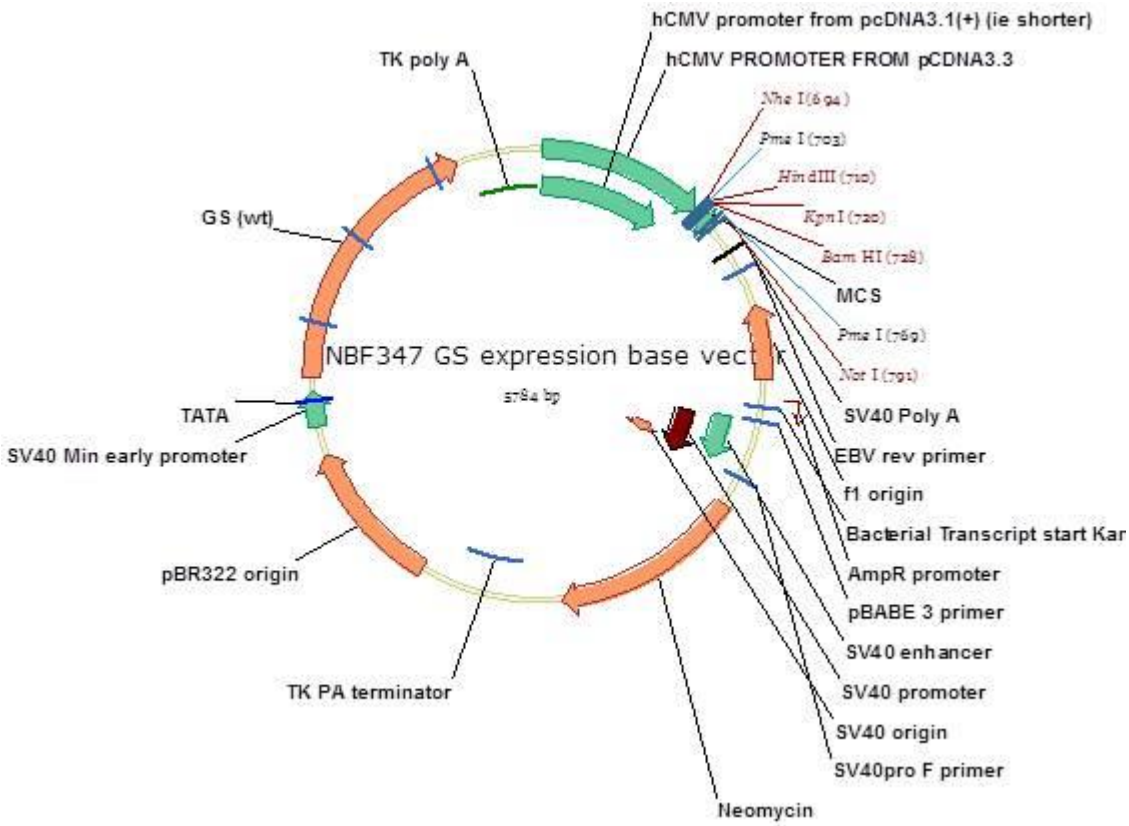

Figure 3: Annotated vector map of plasmid NBF 347.

BsAb genes were inserted between Hind III and NotI restriction sites.

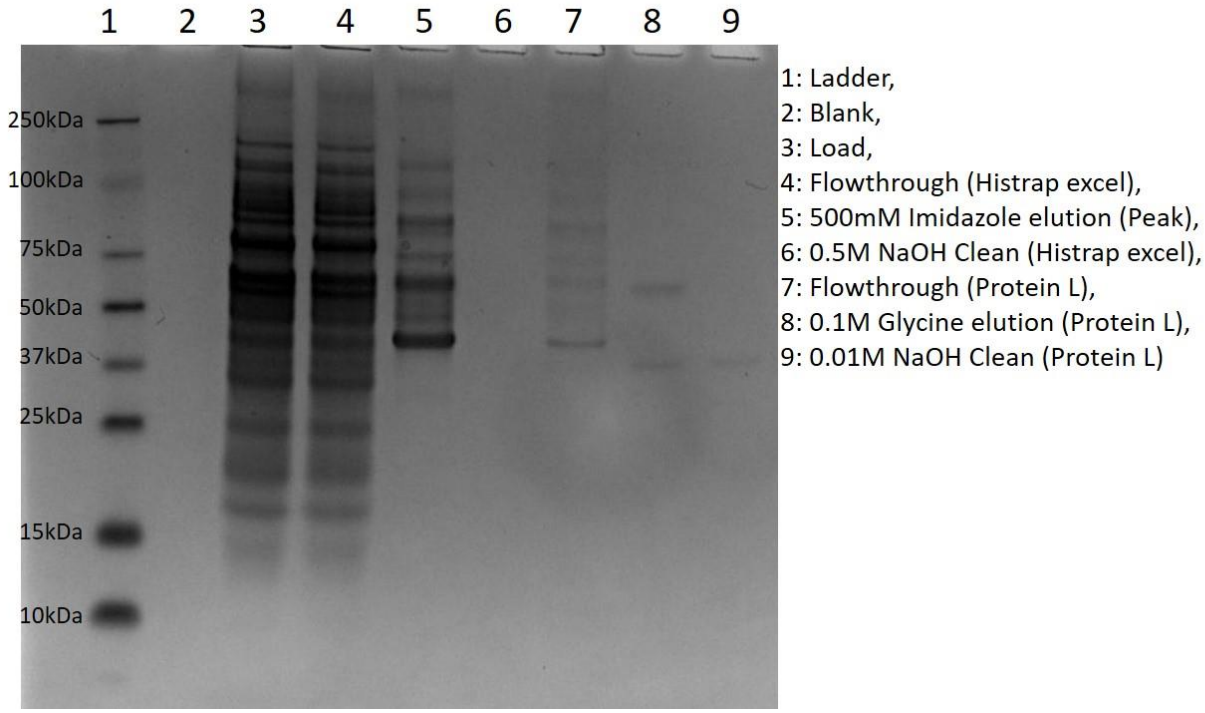

Figure 4: SDS-PAGE gel of anti-EGFR-PEG BsAb purification from CHO cell culture supernatant. Samples were taken sequentially during the purification process and reduced. The gel was run according to standard protocol and shows high BsAb purity (> 99%) following purification with Protein L but not following purification with His trap.

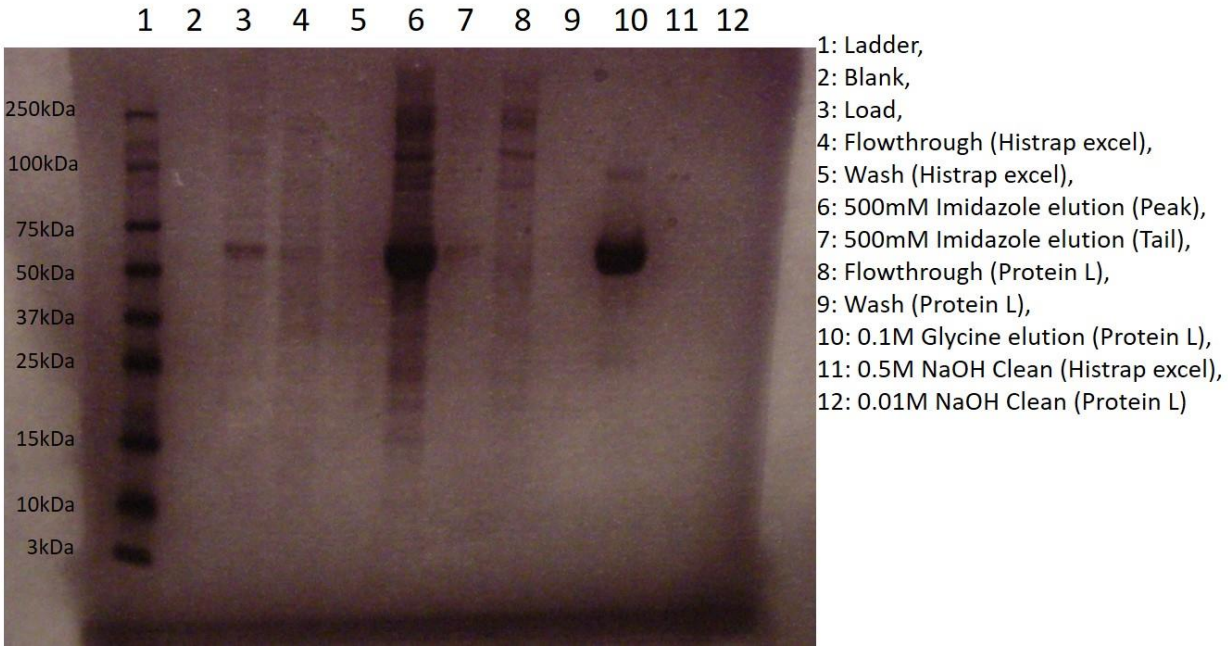

Figure 5: SDS-PAGE gel of anti-CD171-PEG BsAb purification from CHO cell culture supernatant. Samples were taken sequentially during the purification process and reduced. The gel was run according to standard protocol and shows high BsAb purity (> 99%) following purification with Protein L but not following purification with His trap.

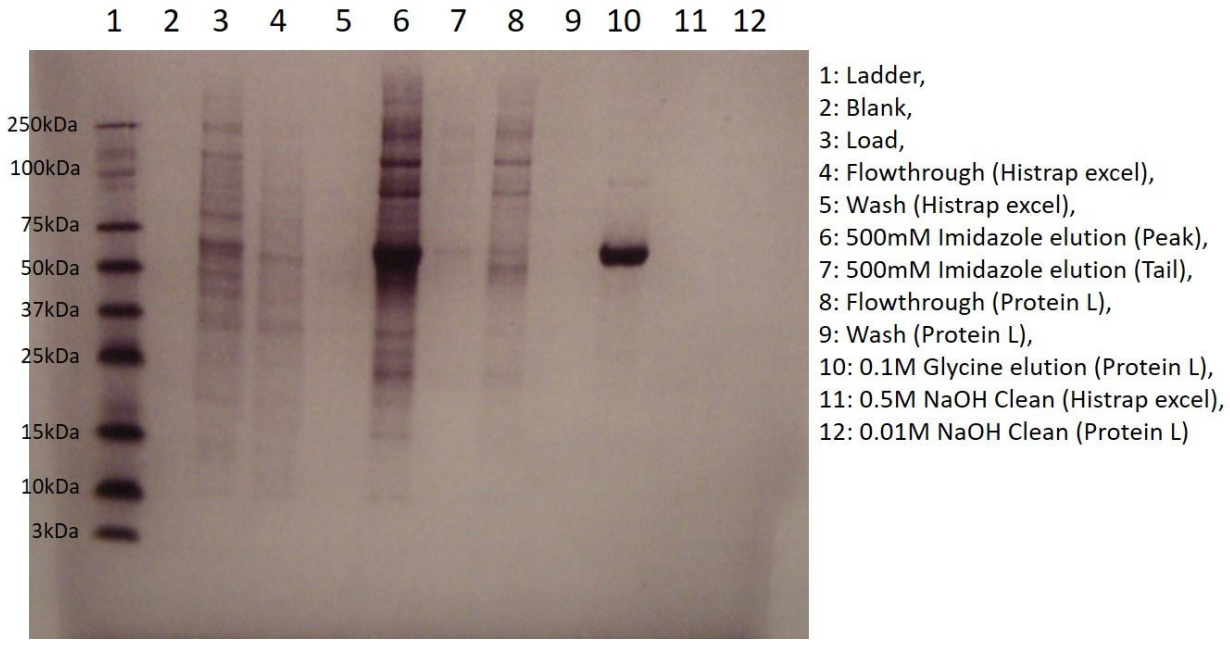

Figure 6: SDS-PAGE gel of anti-CD200-PEG BsAb purification from CHO cell culture supernatant. Samples were taken sequentially during the purification process and reduced. The gel was run according to standard protocol and shows high BsAb purity (> 99%) following purification with Protein L but not following purification with His trap.

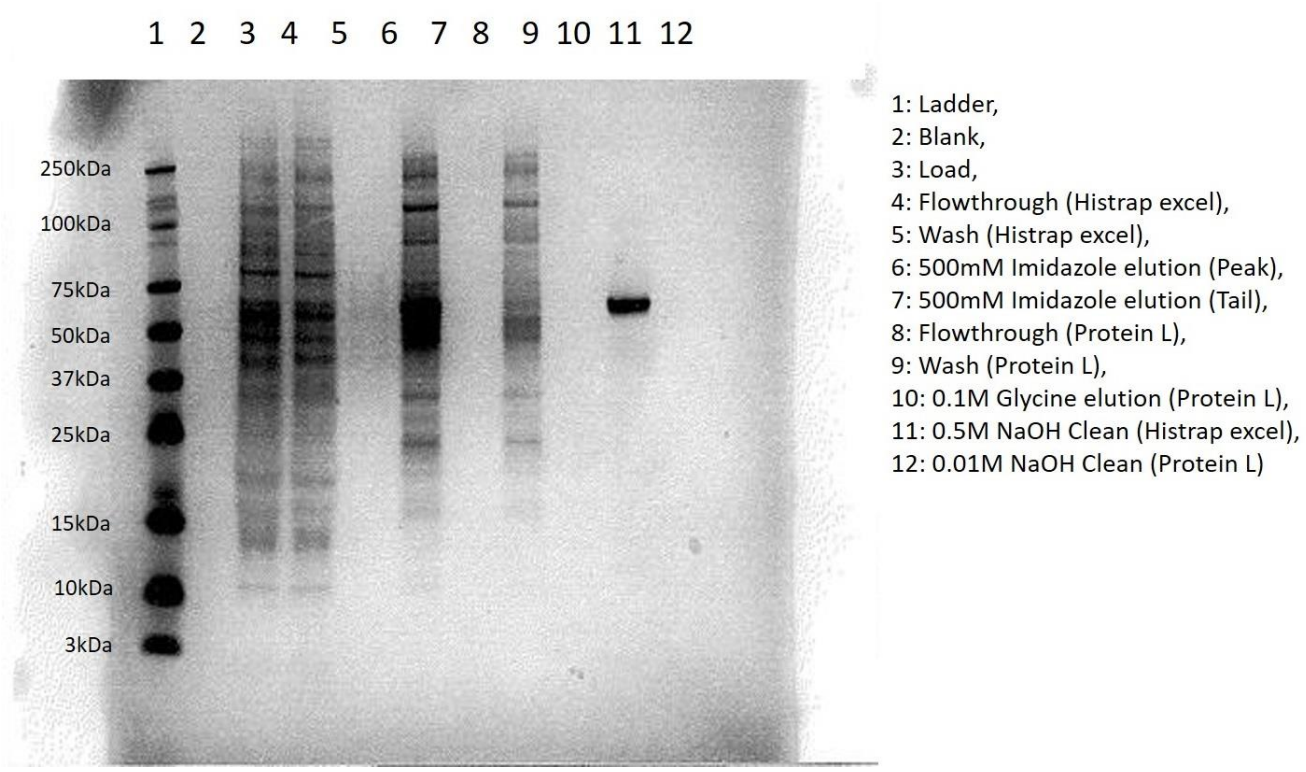

Figure 7: SDS-PAGE gel of anti-CD223-PEG BsAb purification from CHO cell culture supernatant.

Samples were taken sequentially during the purification process and reduced. The gel was run according to standard protocol and shows high BsAb purity (> 99%) following purification with Protein L but not following purification with His trap.

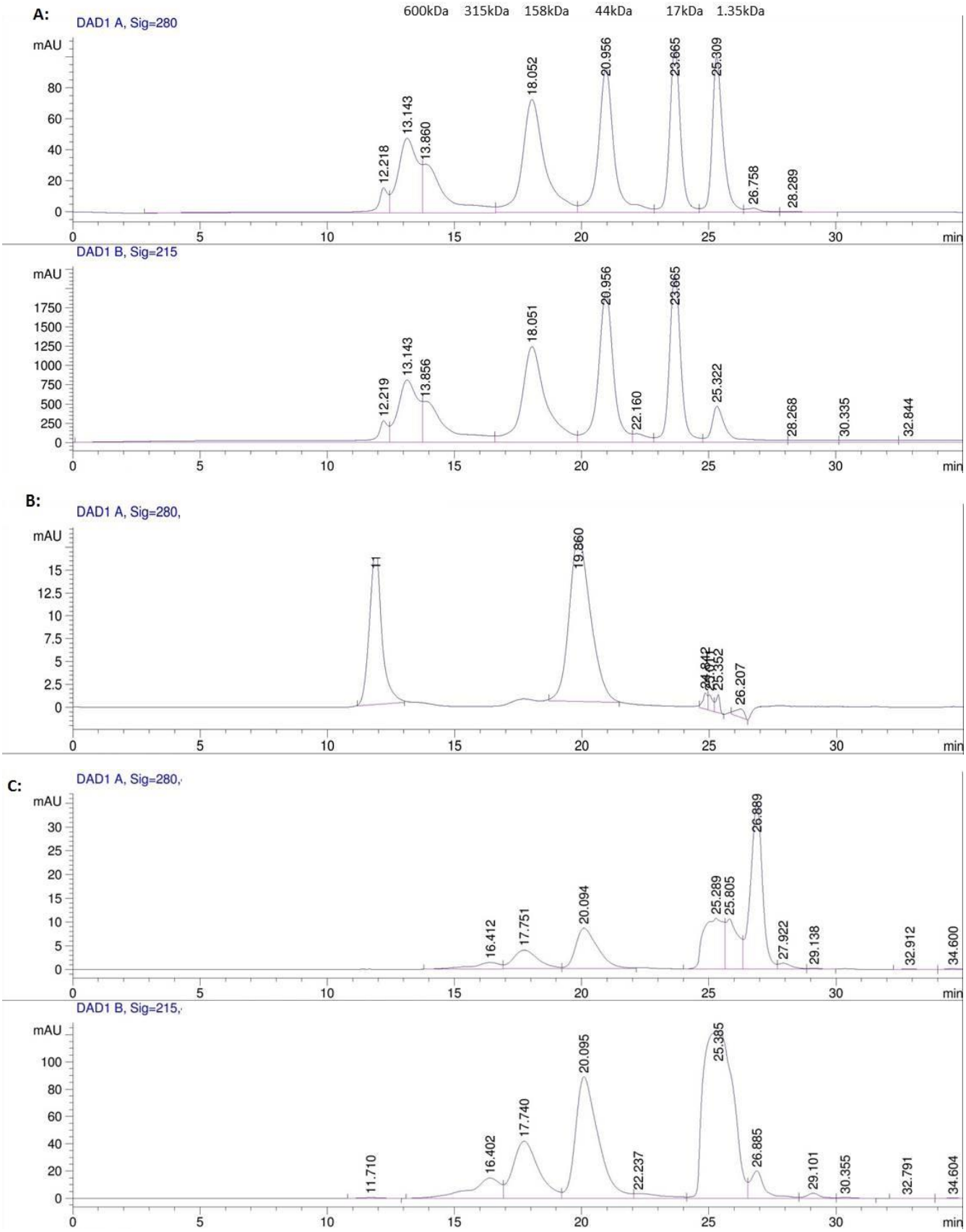
A:
600kDa 315kDa 158kDa 44kDa 17kDa 1.35kDa
DAD1 A, Sig=280
mAU
12.218
13.143
13.860
18.052
20.956
23.665
25.309
26.758
28.289
min
DAD1 B, Sig=215
mAU
12.219
13.143
13.856
18.051
20.956
22.160
23.665
25.322
28.268
30.335
32.844
min
B:
DAD1 A, Sig=280,
mAU
11
19.860
24.842
25.352
26.207
min
C:
DAD1 A, Sig=280,
mAU
16.412
17.751
20.094
25.289
25.805
26.889
27.922
29.138
32.912
34.600
min
DAD1 B, Sig=215,
mAU
11.710
16.402
17.740
20.095
22.237
25.385
26.885
29.101
30.355
32.791
34.604
min

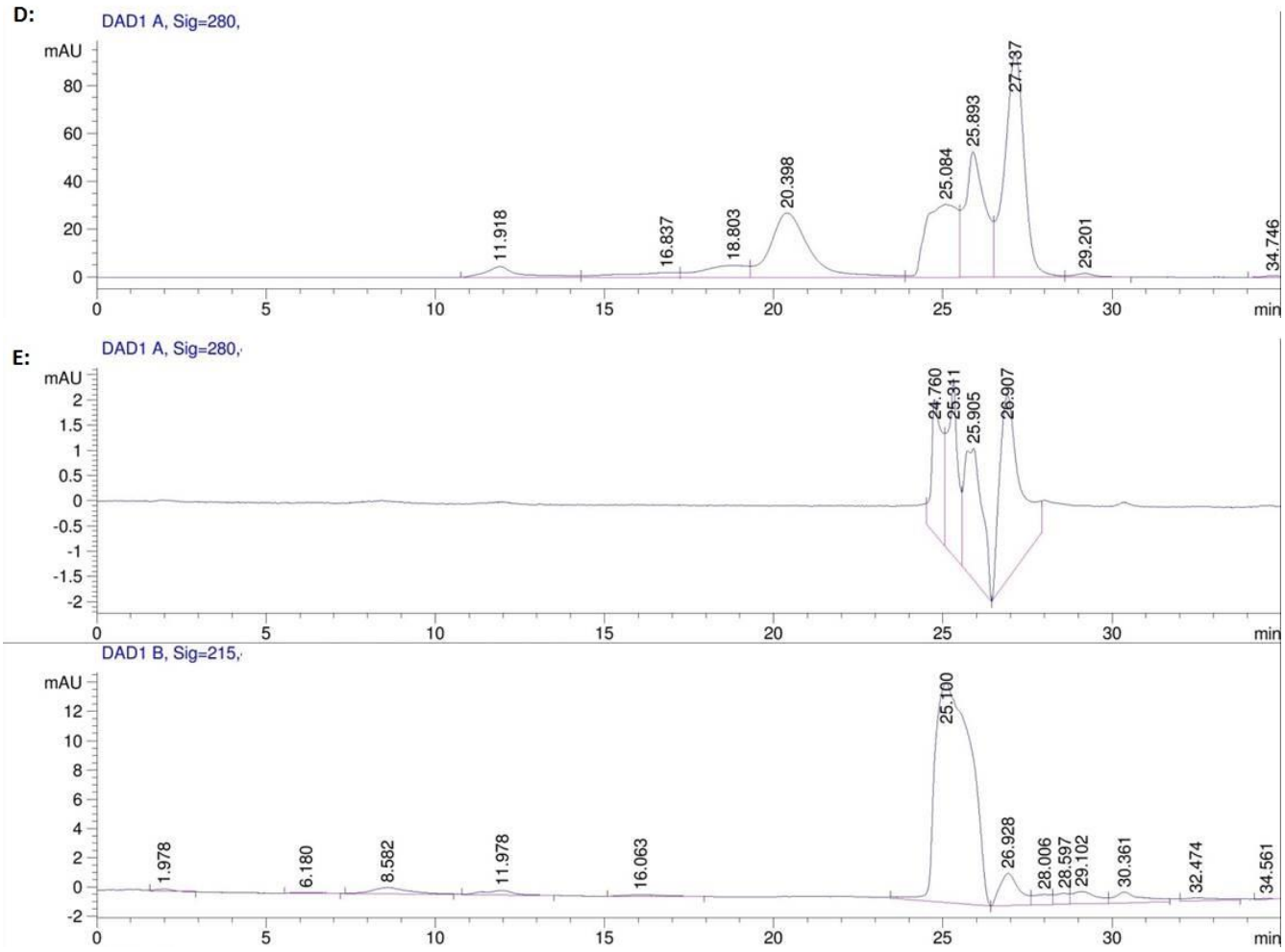

Figure 8: Isocratic size exclusion HPLC of BsAbs.

50µl of BsAb was diluted in PBS and loaded on a Tosoh Biosciences TSKGel G3000SWXL and eluted with 20% Ethanol in PBS. A: Biorad protein standard B: Analysis of anti-EGFR-PEG(15-2) BsAb shows peaks at elution times indicating the presence of high quantities of monomeric antibody (19.9 min) as well as antibody aggregate (11 min) C: Analysis of anti-Cd171-PEG BsAb shows peaks at elution times indicating the presence of high quantities of monomeric (20.1min) as well as some dimeric (17.7 min)) and quadrimeric antibody (16.4min) antibody, but not antibody aggregate. D: Analysis of anti-Cd200-PEG BsAb shows peaks at elution times indicating the presence of high quantities of monomeric (20.4min) as well as some dimeric (18.8 min)) and quadrimeric antibody (16.8min) antibody, as well as some antibody aggregate (11.9min). E: Analysis of anti-Cd223-PEG BsAb shows peaks at elution times indicating the presence of no monomeric or dimeric but quadrimeric antibody (16.0min) as well as multiple aggregate species (11.9min & 8.5min).

A:

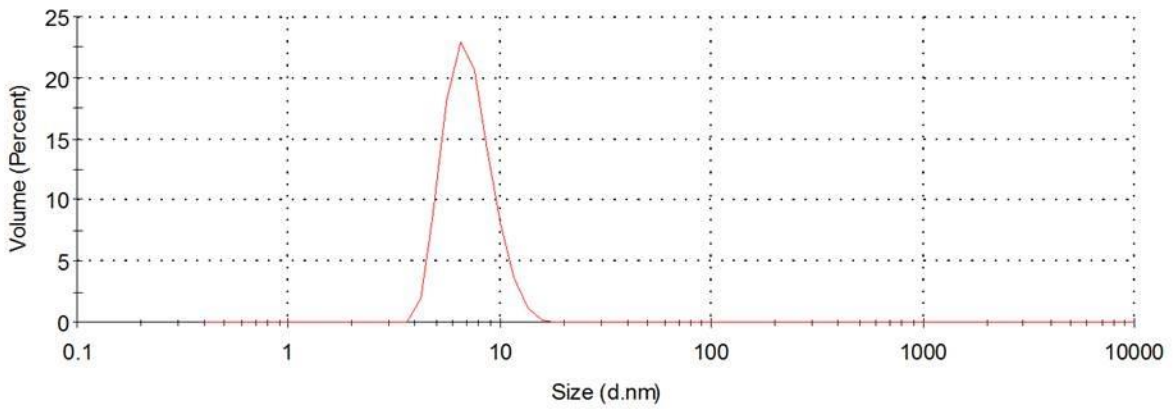
Size Distribution by Volume
Volume (Percent)
25
20
15
10
5
0
0.1
1
10
100
1000
10000
Size (d.nm)

B:

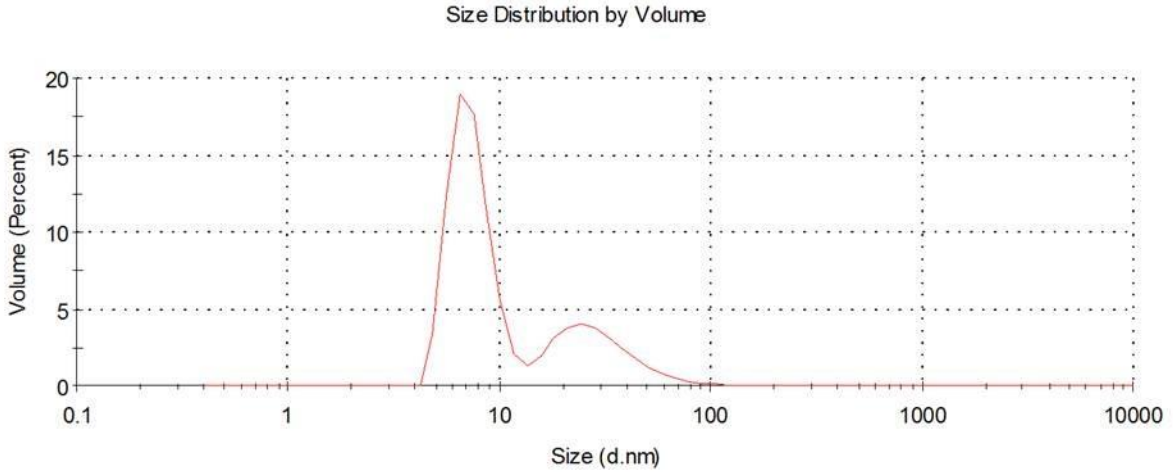
Size Distribution by Volume
Volume (Percent)
20
15
10
5
0
0.1
1
10
100
1000
10000
Size (d.nm)

C:

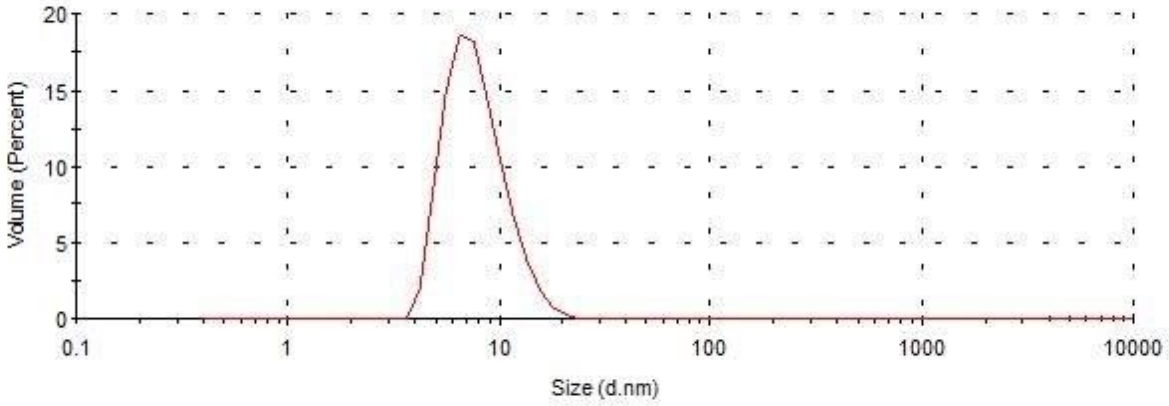
Size Distribution by Volume
Volume (Percent)
20
15
10
5
0
0.1
1
10
100
1000
10000
Size (d.nm)

D:

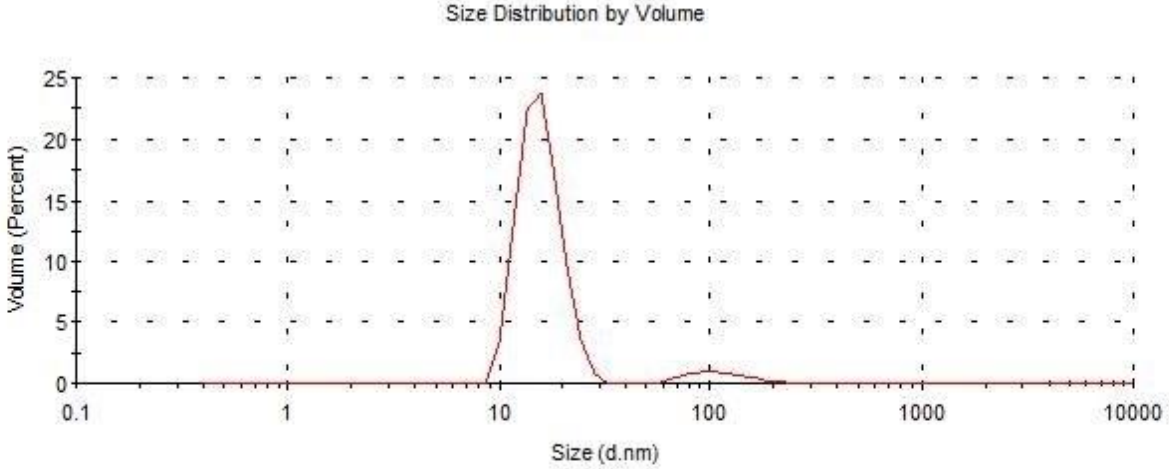
Size Distribution by Volume
Volume (Percent)
25
20
15
10
5
0
0.1
1
10
100
1000
10000
Size (d.nm)

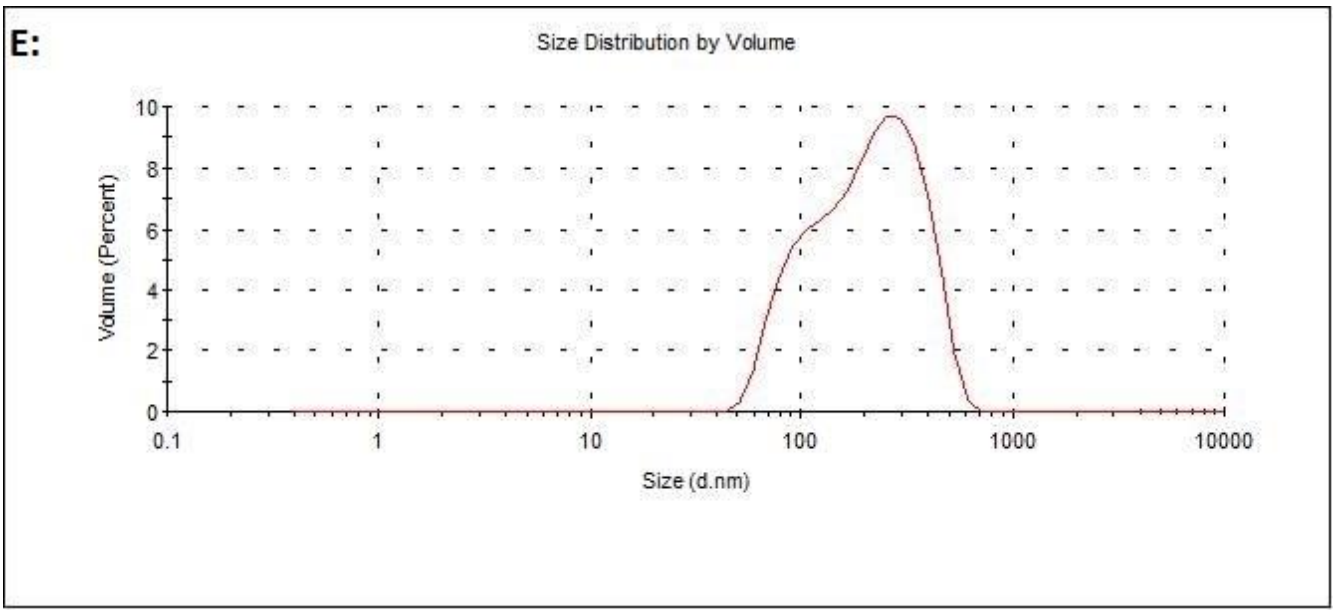

Figure 9: Biospecific Antibody Molecular size distribution determined by Dynamic Light Scatter analysis.

Backscatter angle 173 degrees; Dispersant: 0.5M NaCl 0.1M arginine, dispersant viscosity 0.9286mPa/s, dispersant refractive index 1.349; Sample: Protein, refractive index 1.450, absorbance 0.001. A: anti -EGFR-LPS BsAb is present as 100% monomer in 500mM NaCl 100mM Arginine Buffer. Monomers show a spherical size of 7.261nm +- 1.897nm B: anti -EGFR- PEG (15-2) BsAb is present as a mixture of 72% monomer and 28% aggregate in 500mM NaCl 100mM Arginine Buffer. Monomers show a spherical size of 7.428nm +- 1.763nm. C: anti –CD171-PEG BsAb is present as 100% monomer in 500mM NaCl 100mM Arginine Buffer. Monomers show a spherical size of 8.004nm +- 2.708 nm D: anti–CD200- PEG BsAb is present as a mixture of 94.2% multimer and 5.8% aggregate in 500mM NaCl 100mM Arginine Buffer. Multimers show a spherical size of 15.88nm +- 3.567nm. E: anti –CD223-PEG BsAb is present as 100% aggregate in 500mM NaCl 100mM Arginine Buffer.

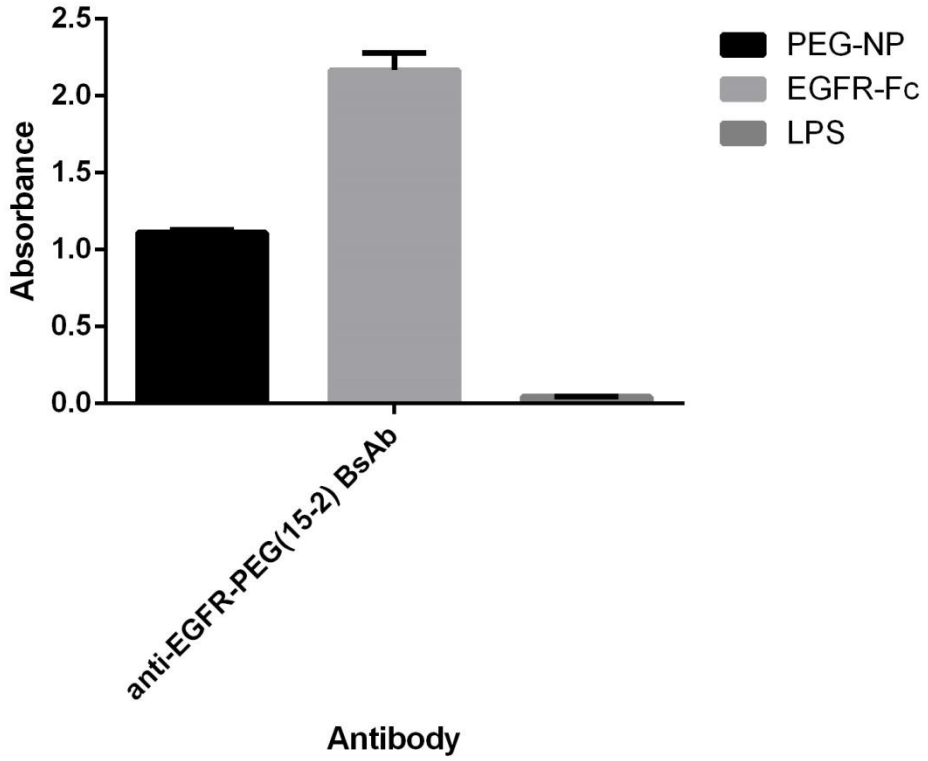

Figure 10: ELISA of anti-EGFR-PEG(15-2) BsAb binding to the immobilized nanoparticle.

96 Well plates were coated with 10μg/ml receptor/nanoparticle and exposed to a concentration of 100μg/ml of BsAb. Binding was assayed using anti-c-myc HRP and TMB. Absorbance readings (450nm) were plotted using Graph Pad Prism. Anti-EGFR-PEG(15-2) BsAb shows specific binding to both EGFR and the methoxyl-PEG-nanoparticle, but not LPS in the absence of Tween 20.

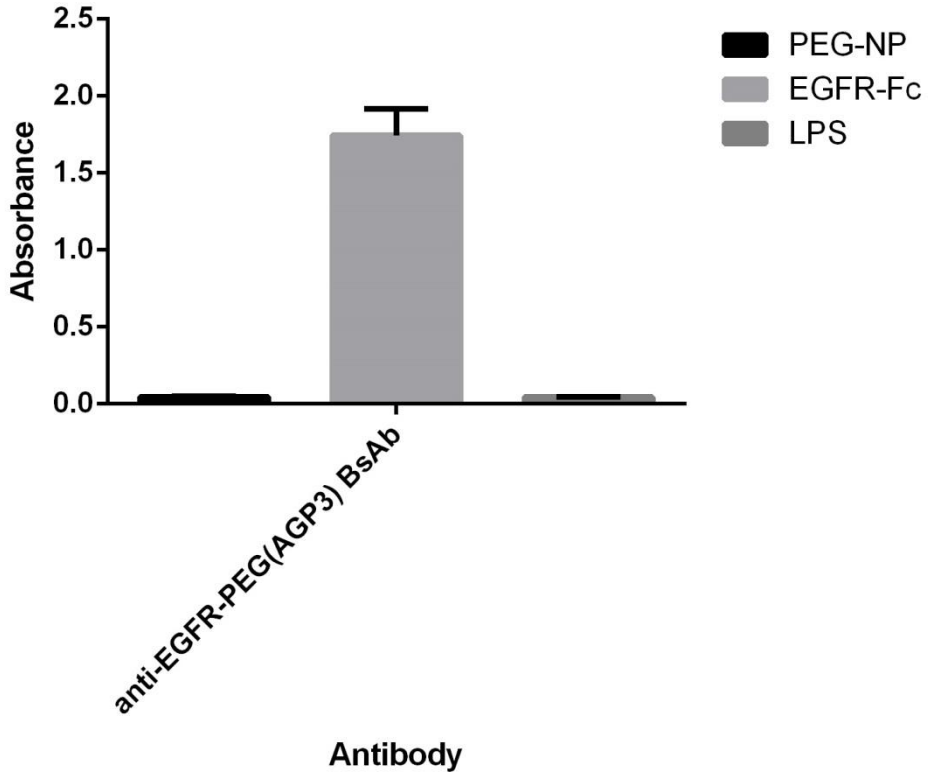

Figure 11: ELISA of anti-EGFR-PEG(AGP3) BsAb binding to the immobilized nanoparticle.

96 Well plates were coated with 10µg/ml receptor/nanoparticle and exposed to a concentration of 100µg/ml of BsAb. Binding was assayed using anti-c-myc HRP and TMB. Absorbance readings (450nm) were plotted using Graph Pad Prism. Anti-EGFR-PEG(AGP3) BsAb shows specific binding to EGFR but neither the methoxyl-PEG-nanoparticle or LPS in the absence of Tween 20.

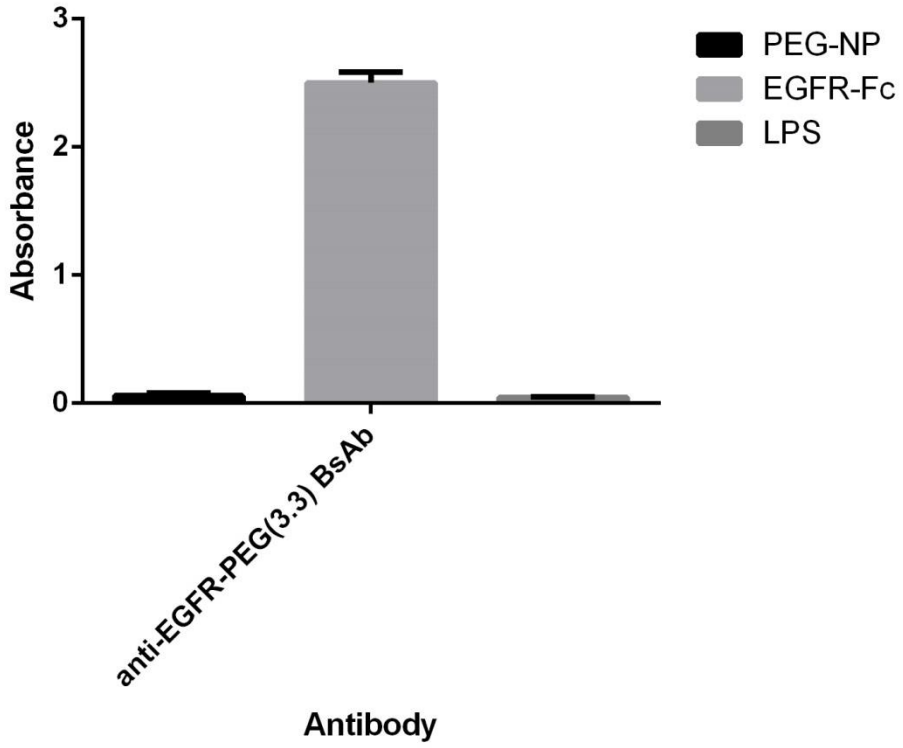

Figure 12: ELISA of anti-EGFR-PEG(3.3) BsAb binding to the immobilized nanoparticle.

96 Well plates were coated with 10μg/ml receptor/nanoparticle and exposed to a concentration of 100μg/ml of BsAb. Binding was assayed using anti-c-myc HRP and TMB. Absorbance readings (450nm) were plotted using Graph Pad Prism. Anti-EGFR-PEG(3.3) BsAb shows specific binding to EGFR but neither the methoxyl-PEG-nanoparticle or LPS in the absence of Tween 20.

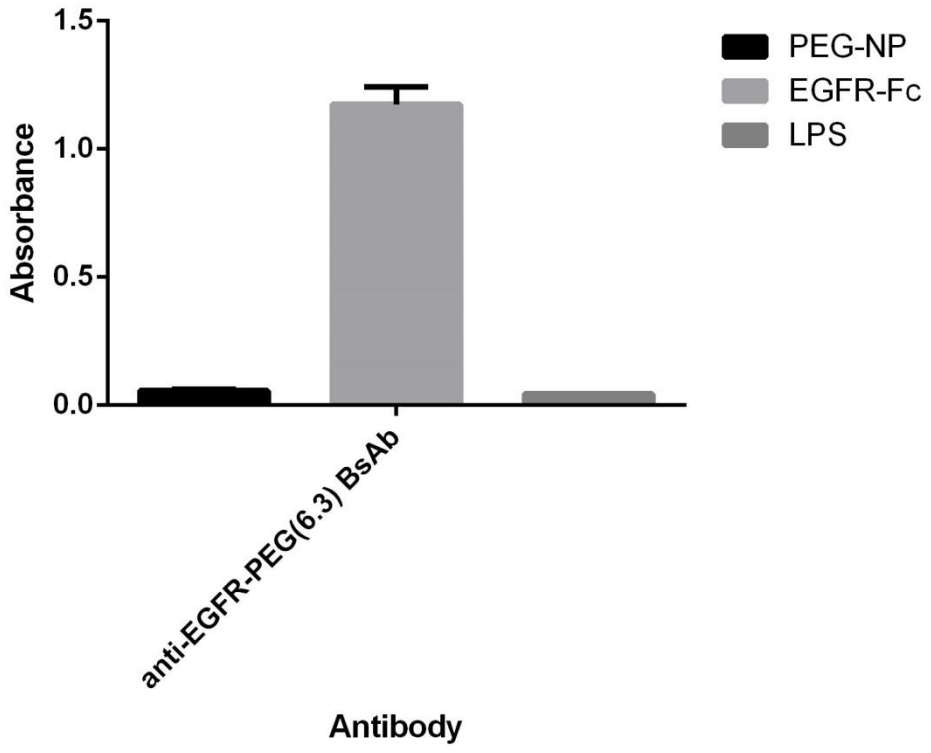

Figure 13: ELISA of anti-EGFR-PEG(6.3) BsAb binding to the immobilized nanoparticle.

96 Well plates were coated with 10μg/ml receptor/nanoparticle and exposed to a concentration of 100μg/ml of BsAb. Binding was assayed using anti-c-myc HRP and TMB. Absorbance readings (450nm) were plotted using Graph Pad Prism. Anti-EGFR-PEG(6.3) BsAb shows specific binding to EGFR but neither the methoxyl-PEG-nanoparticle or LPS in the absence of Tween 20.

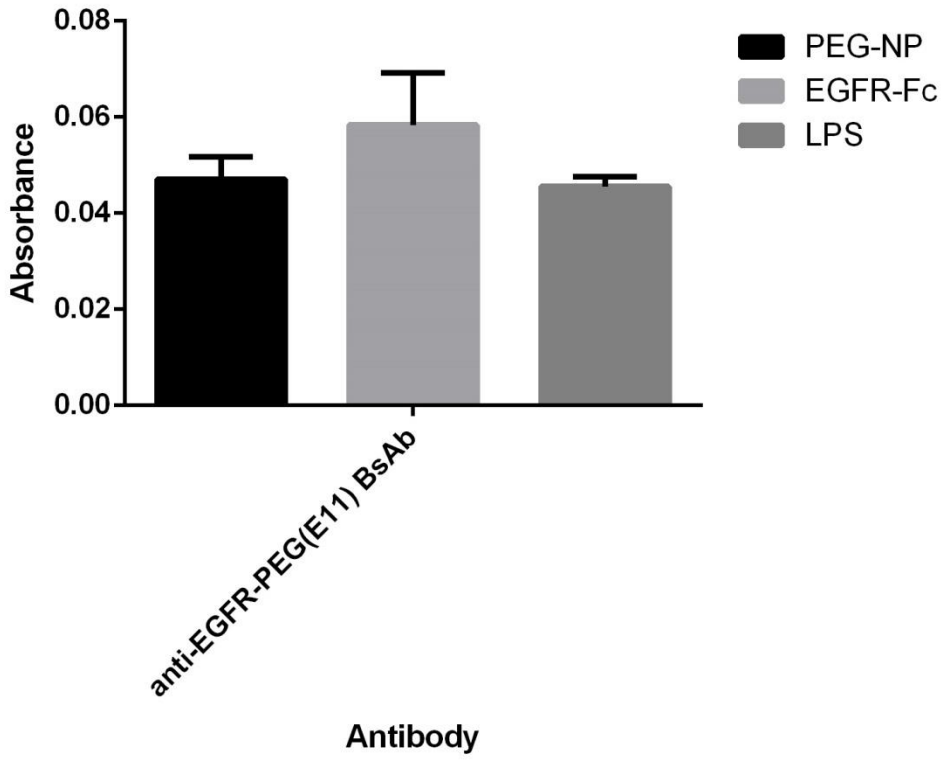

Figure 14: ELISA of anti-EGFR-PEG(E11) BsAb binding to the immobilized nanoparticle.

96 Well plates were coated with 10μg/ml receptor/nanoparticle and exposed to a concentration of 100μg/ml of BsAb. Binding was assayed using anti-c-myc HRP and TMB. Absorbance readings (450nm) were plotted using Graph Pad Prism. Anti-EGFR-PEG(E11) BsAb shows no specific binding to either EGFR, the methoxyl-PEG-nanoparticle or LPS in the absence of Tween 20.

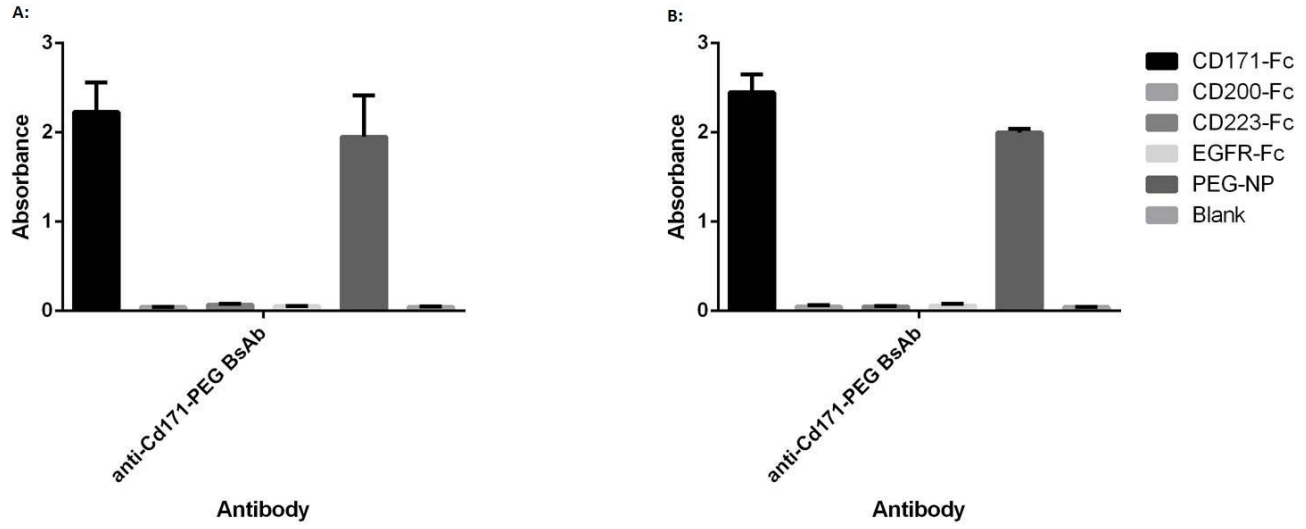

Figure 15: ELISA of anti-CD171-PEG BsAb binding to the immobilized nanoparticle and recombinant receptors.

96 Well plates were coated with 10μg/ml receptor/nanoparticle and exposed to a concentration of 100μg/ml of BsAb. Binding was assayed using anti-c-myc HRP and TMB. Absorbance readings (450nm) were plotted using Graph Pad Prism. Anti-CD171-PEG BsAb shows specific binding to both CD171 and the PEG-nanoparticle in the absence (A) and presence (B) of Tween 20.

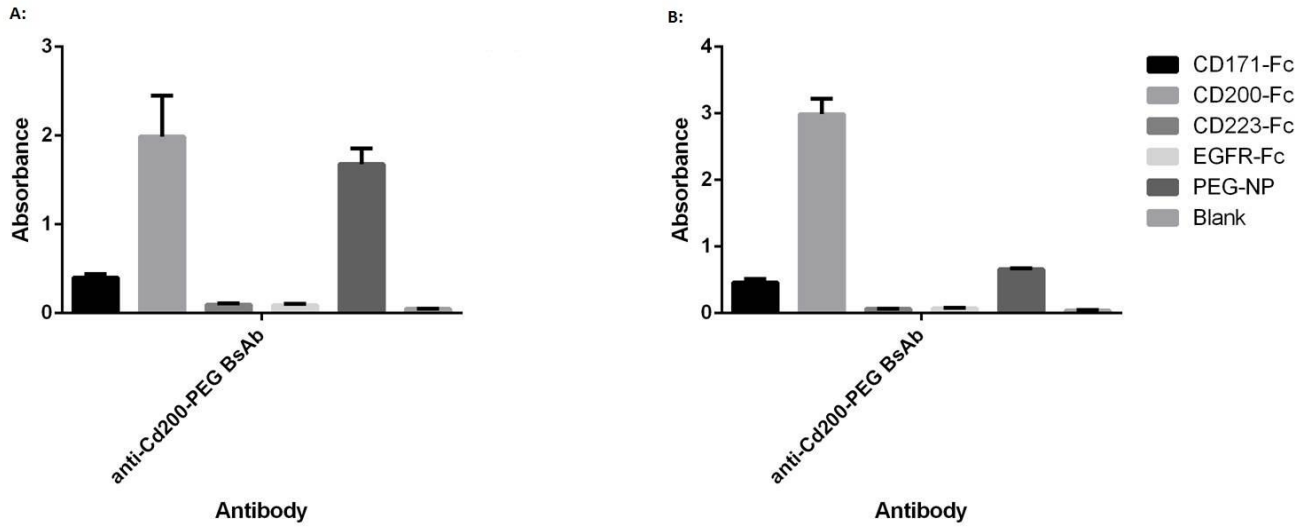

Figure 16: ELISA of anti-CD200-PEG BsAb binding to the immobilized nanoparticle and recombinant receptors.

96 Well plates were coated with 10μg/ml receptor/nanoparticle and exposed to a concentration of 100μg/ml of BsAb. Binding was assayed using anti-c-myc HRP and TMB. Absorbance readings (450nm) were plotted using Graph Pad Prism. Anti-CD200-PEG BsAb shows specific binding to both CD200 and the PEG-nanoparticle in the absence of Tween 20 (A). (B) Binding to PEG-nanoparticle is compromised in the presence of Tween 20.

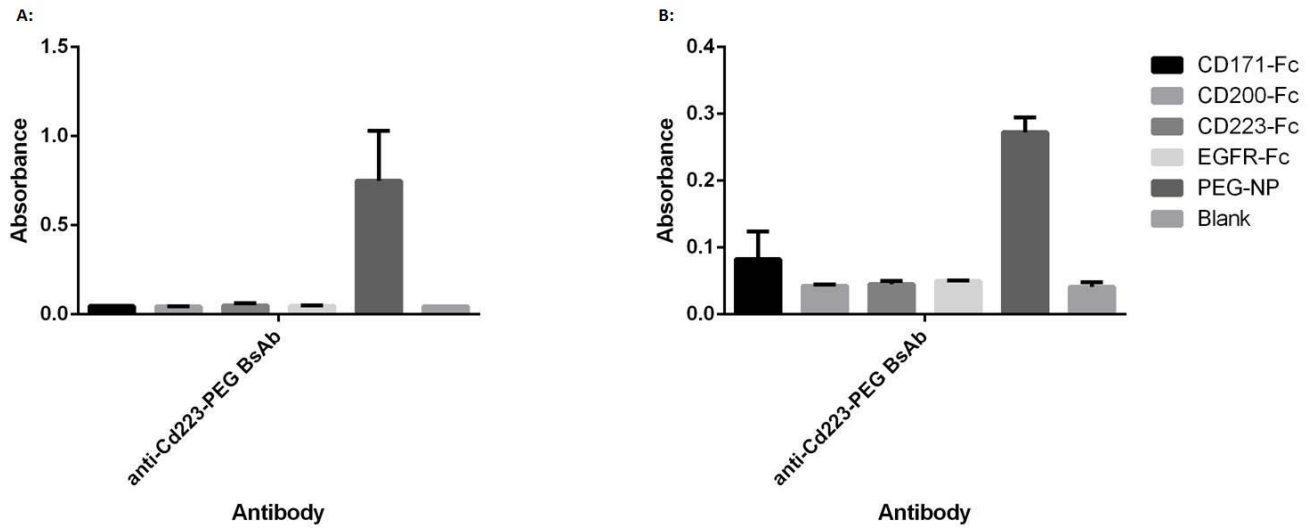

Figure 17: ELISA of anti-CD223-PEG BsAb binding to the immobilized nanoparticle and recombinant receptors.

96 Well plates were coated with 10μg/ml receptor/nanoparticle and exposed to a concentration of 100μg/ml of BsAb. Binding was assayed using anti-c-myc HRP and TMB. Absorbance readings (450nm) were plotted using Graph Pad Prism. Anti-CD223-PEG BsAb shows specific binding to the PEG-nanoparticle, but not CD223 in the absence of Tween 20 (A). (B) Binding to PEG-nanoparticle is compromised in the presence of Tween 20.

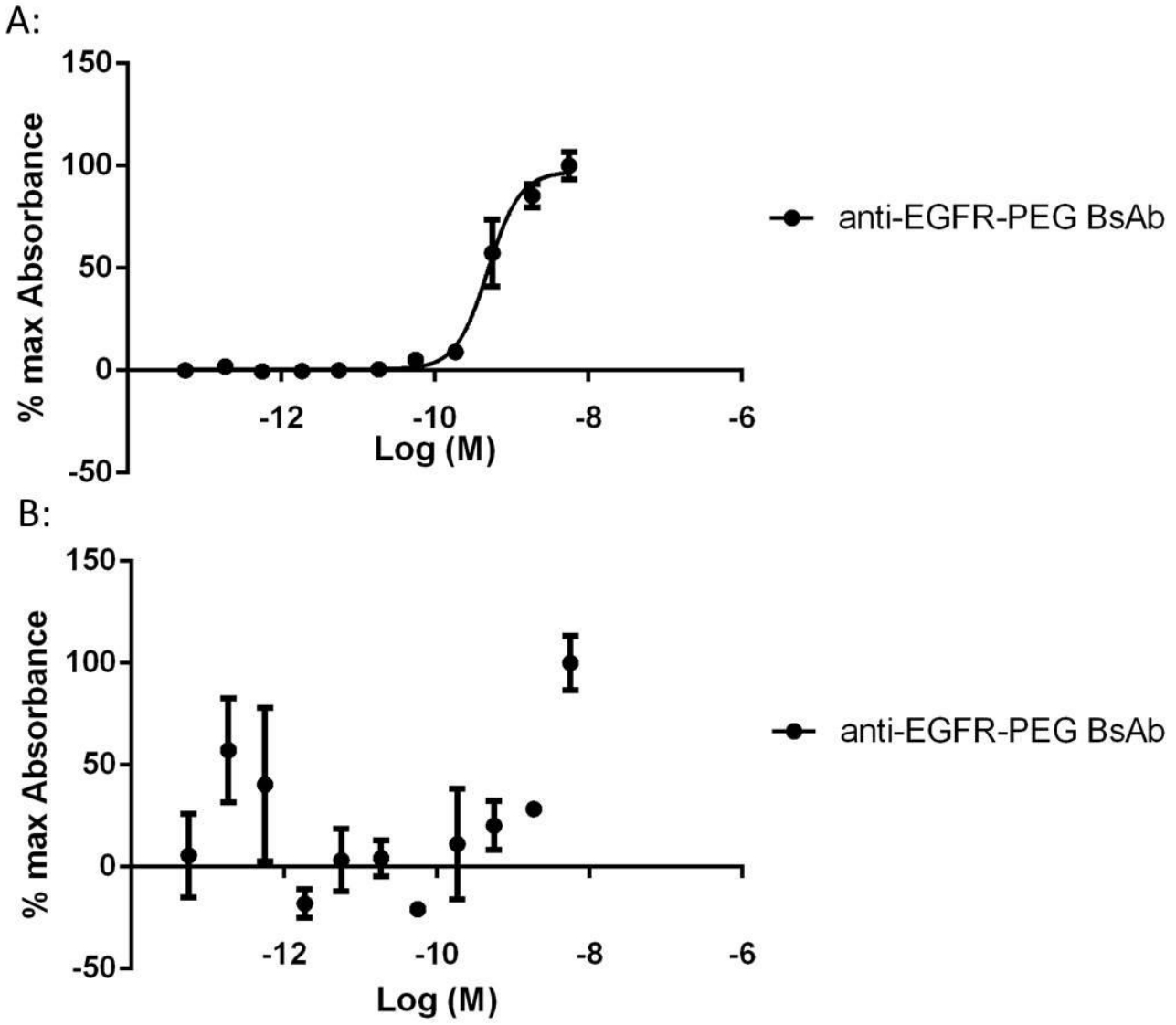

Figure 18: Dose response curve of anti-EGFR-anti-PEG (15-2) BsAb binding to immobilized nanoparticle.

Dose response curve of BsAb binding to immobilized nanoparticle without (A) and with Tween20 (B). 96 Well plates were coated with 10µg/ml Nanoparticle and exposed to a concentration gradient of BsAb. Binding was assayed using anti-c-myc HRP and TMB. Absorbance readings (450nm) were normalized and plotted using Graph Pad Prism. In the absence of Tween20 (A), a line of best fit was calculated using nonlinear regression analysis and was then plotted ($R^2 = 0.9759$). The error is shown as SEM (n=4), from this line of best fit the EC50 was determined to be 490.6 pM +- 70.5pM (A).

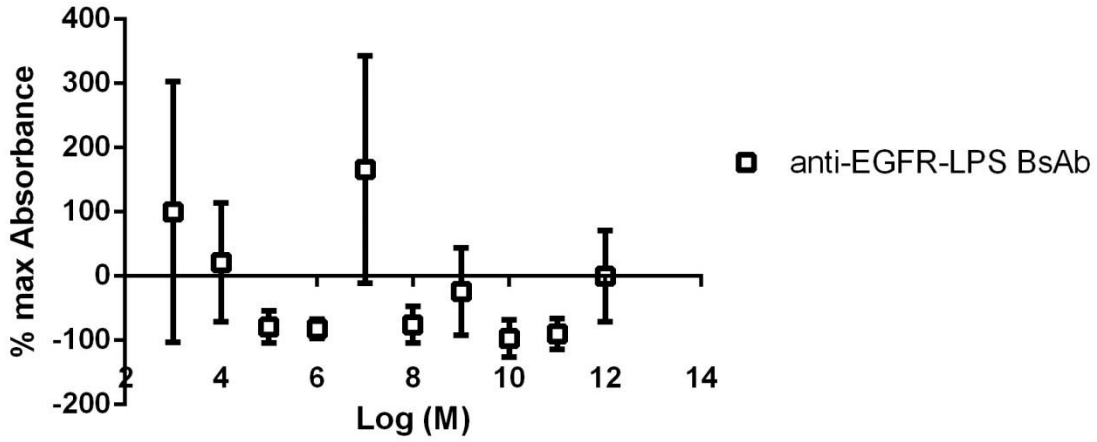

Figure 19: Dose response curve of anti-EGFR-LPS BsAb binding to immobilized nanoparticle.

Dose response curve of BsAb binding to immobilized nanoparticle without Tween20. 96 Well plates were coated with 10μg/ml Nanoparticle and exposed to a concentration gradient of BsAb. Binding was assayed using anti-c-myc HRP and TMB. Absorbance readings (450nm) were normalized and plotted using Graph Pad Prism. No line of best fit could be calculated using nonlinear regression analysis Error shown as SEM (n=4). Results are indicative of no affinity of anti-EGFR-LPS BsAb towards immobilized PEG nanoparticle.

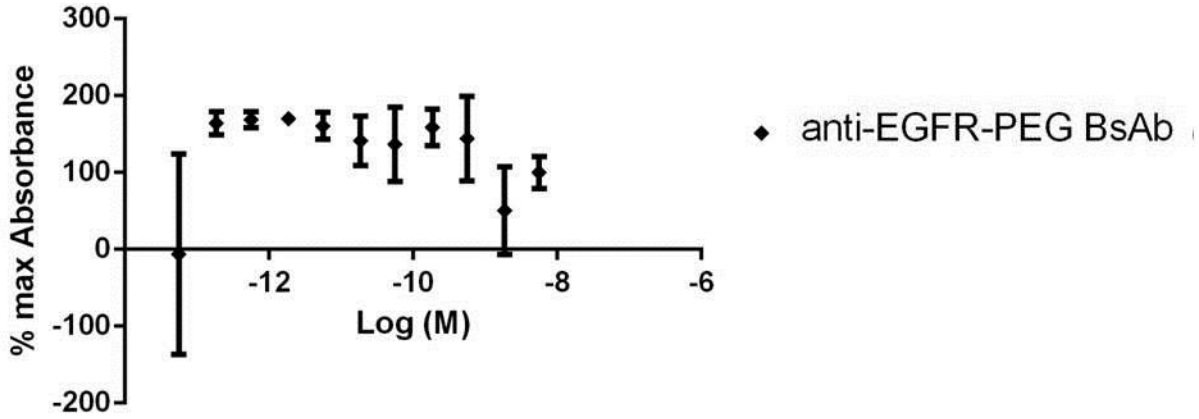

Figure 20: Dose response curve of anti-EGFR-anti-PEG (AGP3) BsAb binding to immobilized nanoparticle.

Dose response curve of BsAb binding to immobilized nanoparticle without Tween20. 96 Well plates were coated with 10μg/ml Nanoparticle and exposed to a concentration gradient of BsAb. Binding was assayed using anti-c-myc HRP and TMB. Absorbance readings (450nm) were normalized and plotted using Graph Pad Prism. No line of best fit could be calculated using nonlinear regression analysis Error shown as SEM (n=4). Results are indicative of no affinity of AGP3 towards immobilized PEG nanoparticle.

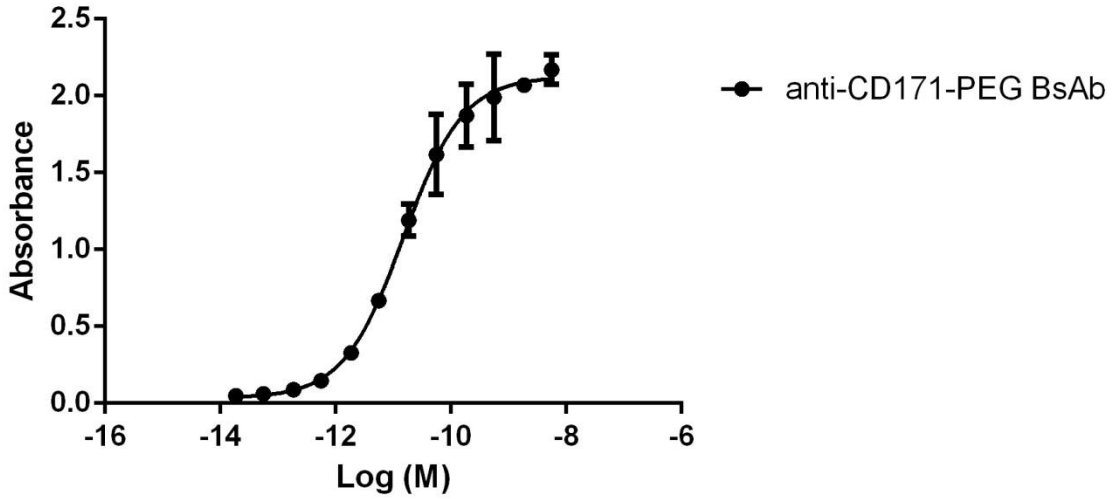

Figure 21: Dose response curve of anti-CD171-PEG BsAb binding to immobilized nanoparticle.

Dose response curve of anti-CD171-PEG BsAb binding to the immobilized recombinant Cd171 receptor with Tween20. 96 Well plates were coated with 10μg/ml recombinant CD171 and exposed to a concentration gradient of BsAb. Binding was assayed using anti-c-myc HRP and TMB. Absorbance readings (450nm) were plotted using Graph Pad Prism. A line of best fit was calculated using nonlinear regression analysis and was then plotted (R2 = 0.9831). Error shown as SD, from this line of best fit the EC50 was determined to be 14.97pM +- 4.16pM.

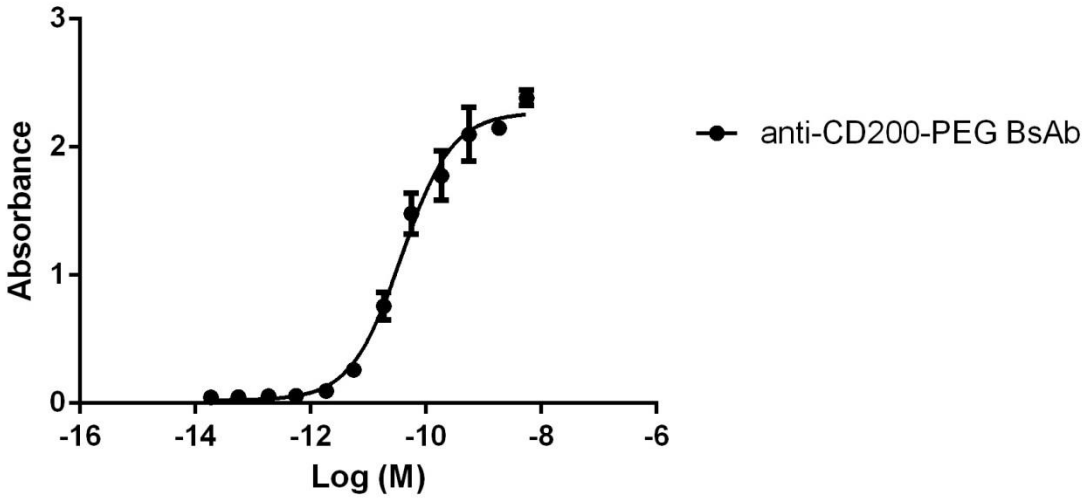

Figure 22: Dose response curve of anti-CD200-PEG BsAb binding to immobilized nanoparticle.

Dose response curve of BsAb binding to immobilized recombinant Cd200 receptor with Tween20. 96 Well plates were coated with 10μg/ml recombinant CD200 and exposed to a concentration gradient of BsAb. Binding was assayed using anti-c-myc HRP and TMB. Absorbance readings (450nm) were plotted using Graph Pad Prism. A line of best fit was calculated using nonlinear regression analysis and was then plotted ($R^2 = 0.9866$). Error shown as SD, from this line of best fit the EC50 was determined to be 37.66pM +- 8.25pM.

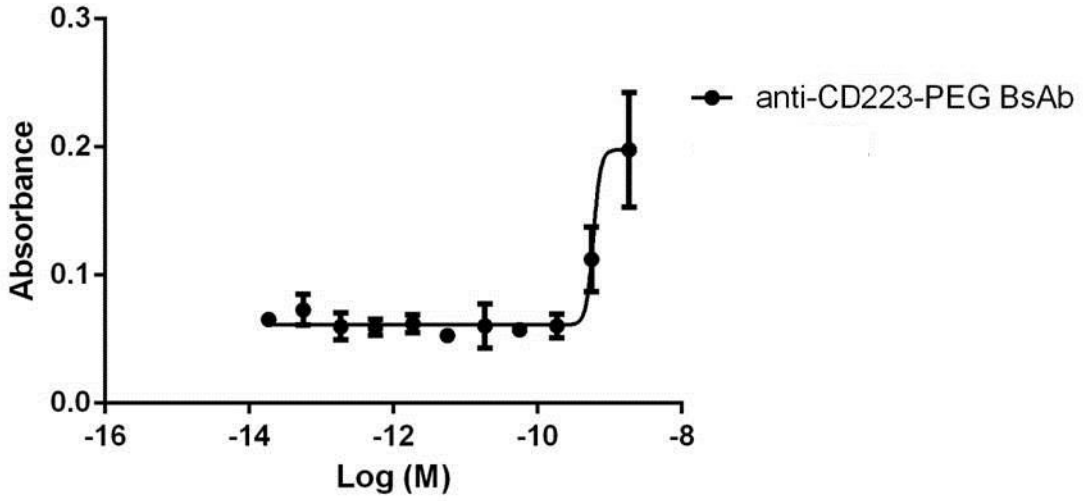

Figure 23: Dose response curve of anti-CD223-PEG BsAb binding to immobilized nanoparticle.

Dose response curve of BsAb binding to the immobilized recombinant Cd223 receptor with Tween20. 96 Well plates were coated with 10μg/ml recombinant CD223 and exposed to a concentration gradient of BsAb. Binding was assayed using anti-c-myc HRP and TMB. Absorbance readings (450nm) were plotted using Graph Pad Prism. A line of best fit was calculated using nonlinear regression analysis and was then plotted (R2 = 0.8789). The error is shown as SD, from this line of best fit the EC50 was determined to be approximately 59.66nM.

PEG:

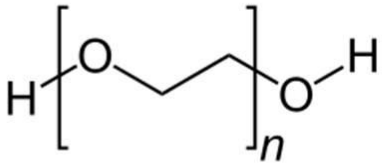

Tween 20:

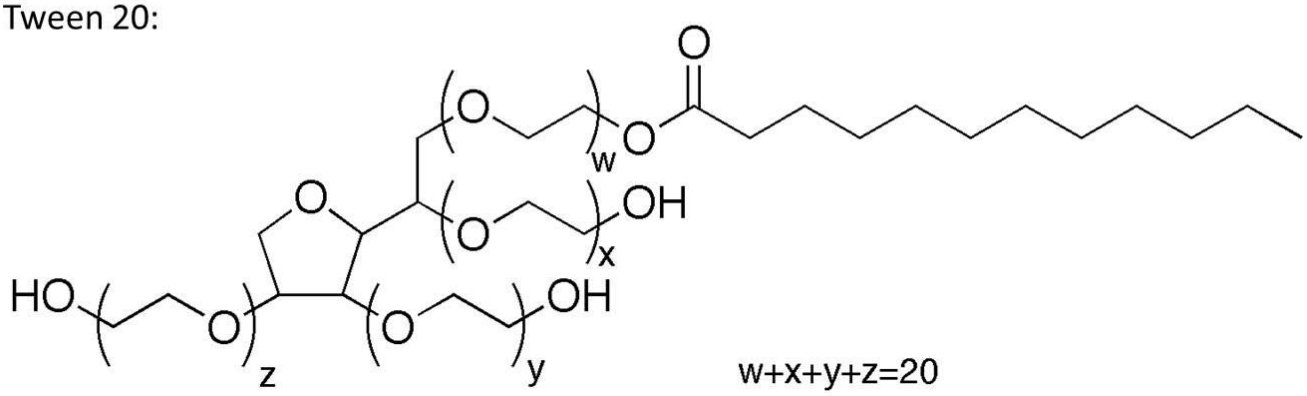

Figure 24: Structural comparison between PEG monomer and Tween 20.

Structural comparison between PEG indicates the presence of 20 PEG-backbone binding sites within the Tween 20 molecule

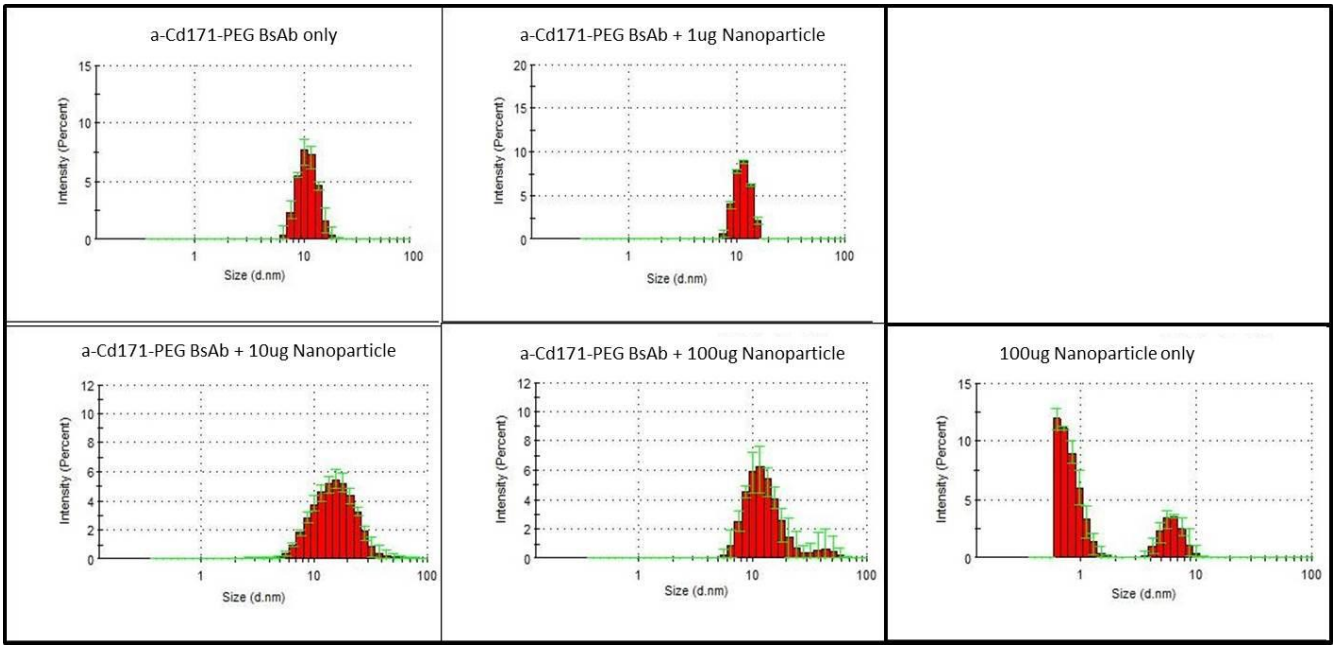

Figure 25: Anti-CD171-PEG BsAb PEG-nanoparticle interaction analysis by Dynamic Light Scatter analysis.

Backscatter angle 173 degrees; Dispersant: 0.5M NaCl 0.1M arginine, dispersant viscosity 0.9286mPa/s, dispersant refractive index 1.349; Sample: Protein, refractive index 1.450, absorbance 0.001. Addition of PEG-Nanoparticle to anti-Cd171-PEG BsAb correlates in a dose-dependent manner with an increase in average particle size (d.nm) , anti-Cd171-PEG BsAb only (10.1nm), anti-Cd171-PEG BsAb + 1µg Nanoparticle (11.7nm), anti-Cd171-PEG BsAb + 10µg Nanoparticle (15.7), anti-Cd171-PEG BsAb + 100µg nanoparticle (11.3 & 43.8) and 100µg Nanoparticle only(5.9). This is indicative of binding of nanoparticle and BsAb.

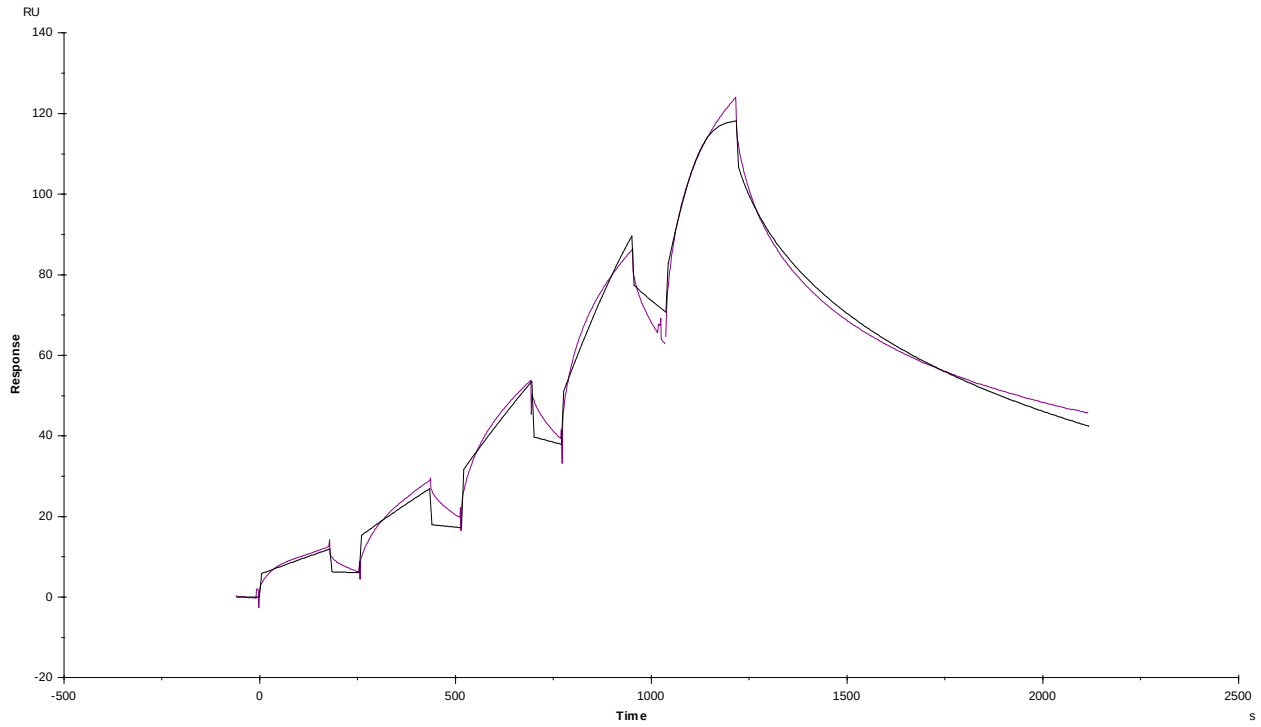

Figure 26: Cd171-hFc anti-Cd171-PEG BsAb Kinetics Assay.

Biacore T200 trace demonstrating the binding of concentrations of anti-Cd171-PEG BsAb ranging from 3.68x10-6M to 2.3x10-7M) to 1000RU immobilized to Cd171-hFc. Analysis with Biacore control software (v2.0) using an assumed 1:1 binding ratio yielded in a calculated K_D of $3.45x10^{-7}$ with a k_a of $2.30x10^{+4}$ and a k_d of $7.94x10^{-3}$.

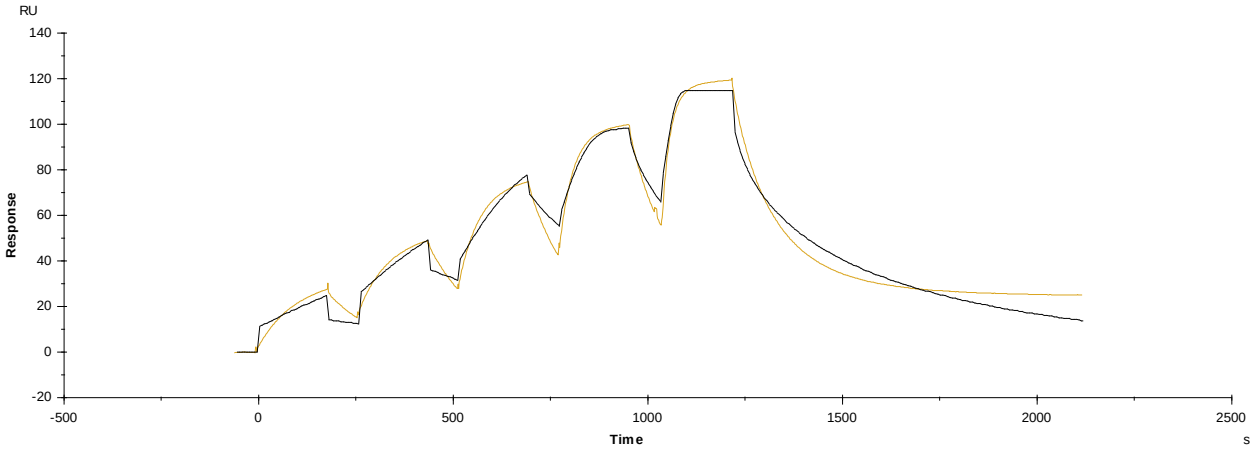

Figure 27: Cd200-hFc anti-Cd200-PEG BsAb Kinetics Assay.

Biacore T200 trace demonstrating the binding of concentrations of anti-Cd200-PEG BsAb ranging from 3.68x10-6M to 2.3x10-7M) to 1000RU immobilized to Cd200-hFc. Analysis with Biacore control software (v2.0) using an assumed 1:1 binding ratio yielded in a calculated K_D of $1.20x10^{-8}$ with a k_a of $4.32x10^{+8}$ and a k_d of 5.2.

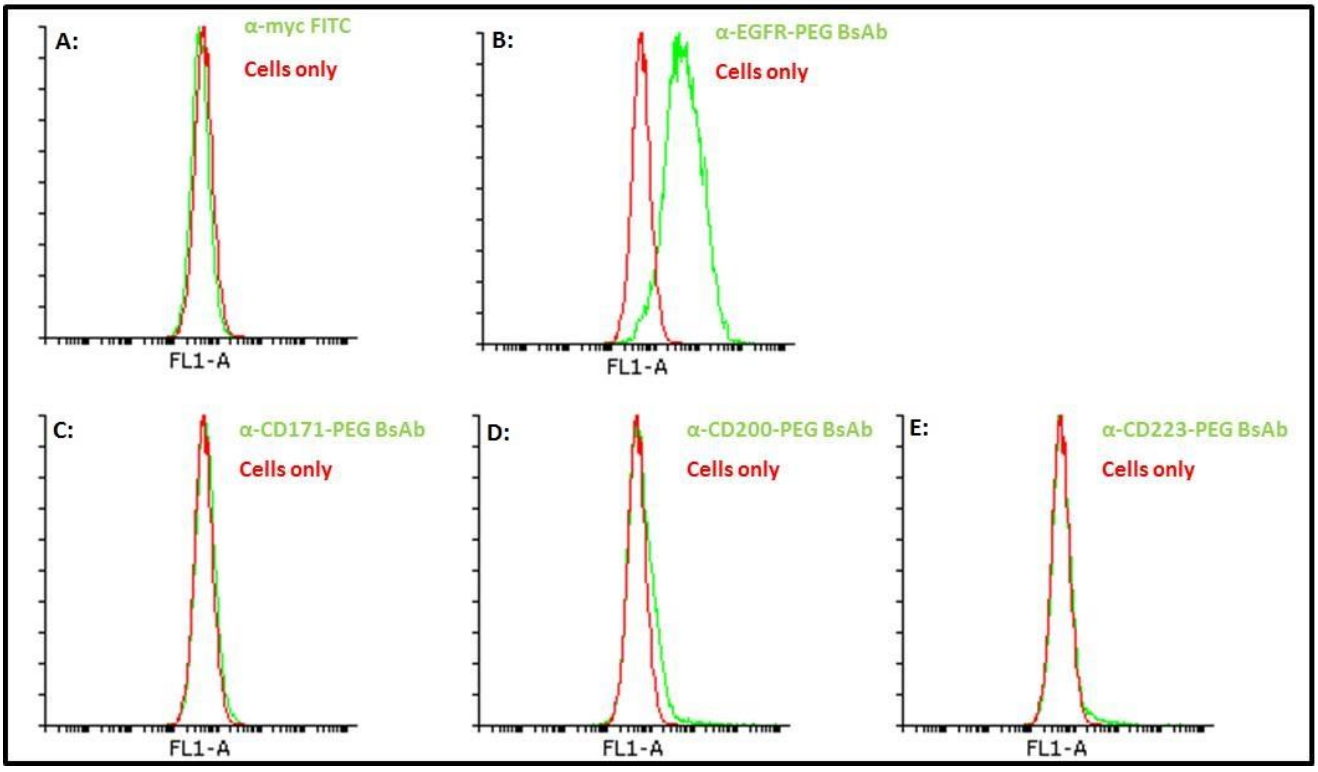

Figure 28: Flow cytometry analysis of anti-myc FITC labelled BsAb binding to MDAMB 468.

MDAMB468 cells were grown to confluency in Advanced RPMI 1640 medium supplemented with 1x Glutamax and 10% FCS and then scraped. Cells were then incubated for 1 hour on ice with either anti-c-myc FITC, anti-c-myc FITC and anti-EGFR-PEG BsAb, anti-c-myc FITC and anti-CD171-PEG BsAb, anti-c-myc FITC and anti-CD200-PEG BsAb or anti-c-myc FITC and anti-CD223-PEG BsAb in PBSFCS (PBS + 10% FCS). Following incubation, cells were washed with PBSFCS to remove unbound antibody and nanoparticle. Fluorescence was then assayed using a BD LSR II Analyser and data was analysed using Flowing 2.1. Panel A (Count / Absorbance 530nm) shows no shift in FITC fluorescence, in the presence of anti-myc FITC antibody alone. Panel B (Count / Absorbance 530nm) shows no shift in FITC fluorescence, in the presence of anti-myc FITC antibody and anti-EGFR-PEG BsAb. This is indicative of binding of BsAb to cells. Panel C (Count / Absorbance 530nm) shows no shift in FITC fluorescence, in the presence of anti-myc FITC antibody and anti-CD171-PEG BsAb. Panel D (Count / Absorbance 530nm)) shows no shift in FITC fluorescence, in the presence of anti-myc FITC antibody and anti-CD200-PEG BsAb. Panel E (Count / Absorbance 530nm)) shows no shift in FITC fluorescence, in the presence of anti-myc FITC antibody and anti-CD223-PEG BsAb.

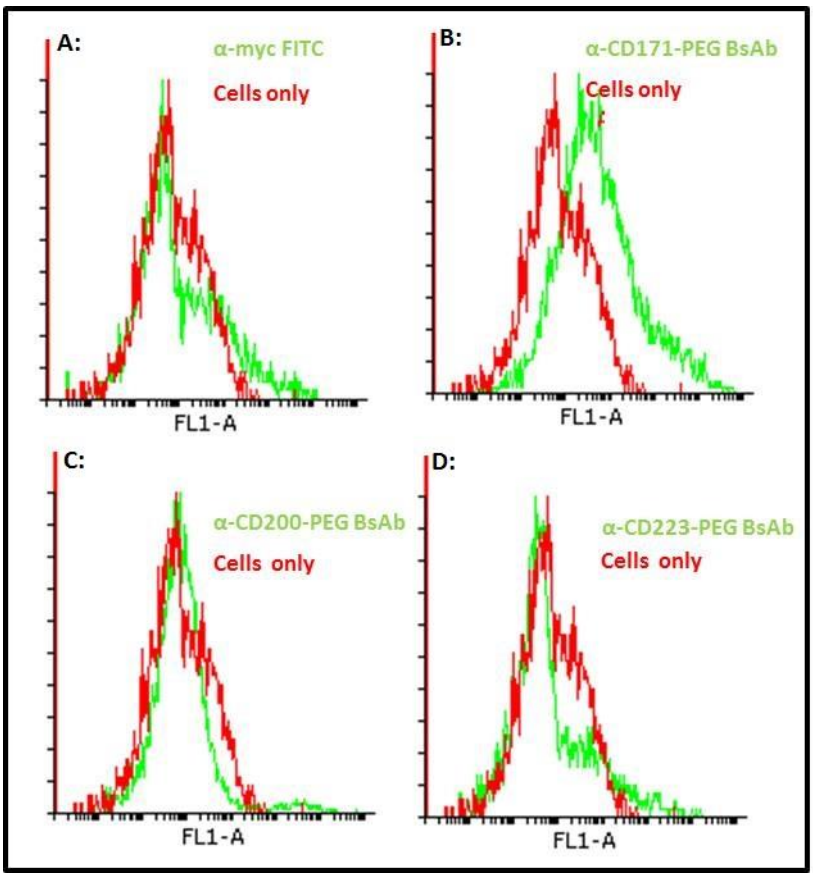

Figure 29: Flow cytometry analysis of anti-myc FITC labelled BsAb binding to SKOV-3.

SKOV-3 cells were grown to confluency in Advanced RPMI 1640 medium supplemented with 1x Glutamax and 10% FCS and then scraped. Cells were then incubated for 1 hour on ice with either anti-c-myc FITC, anti-c-myc FITC and anti-CD171-PEG BsAb, anti-c-myc FITC and anti-CD200-PEG BsAb or anti-c-myc FITC and anti-CD223-PEG BsAb in PBSFCS (PBS + 10% FCS). Following incubation, cells were washed with PBSFCS to remove unbound antibody and nanoparticle. Fluorescence was then assayed using a BD LSR II Analyser and data was analysed using Flowing 2.1. Panel A (Count / Absorbance 530nm) shows no shift in FITC fluorescence, in the presence of anti-myc FITC antibody alone. Panel B (Count / Absorbance 530nm) shows a shift in FITC fluorescence, in the presence of anti-myc FITC antibody and anti-CD171-PEG BsAb. This is indicative of BsAb binding to the cell. Panel C (Count / Absorbance 530nm)) shows no shift in FITC fluorescence, in the presence of anti-myc FITC antibody and anti-CD200-PEG BsAb. Panel D (Count / Absorbance 530nm)) shows no shift in FITC fluorescence, in the presence of anti-myc FITC antibody and anti-CD223-PEG BsAb.

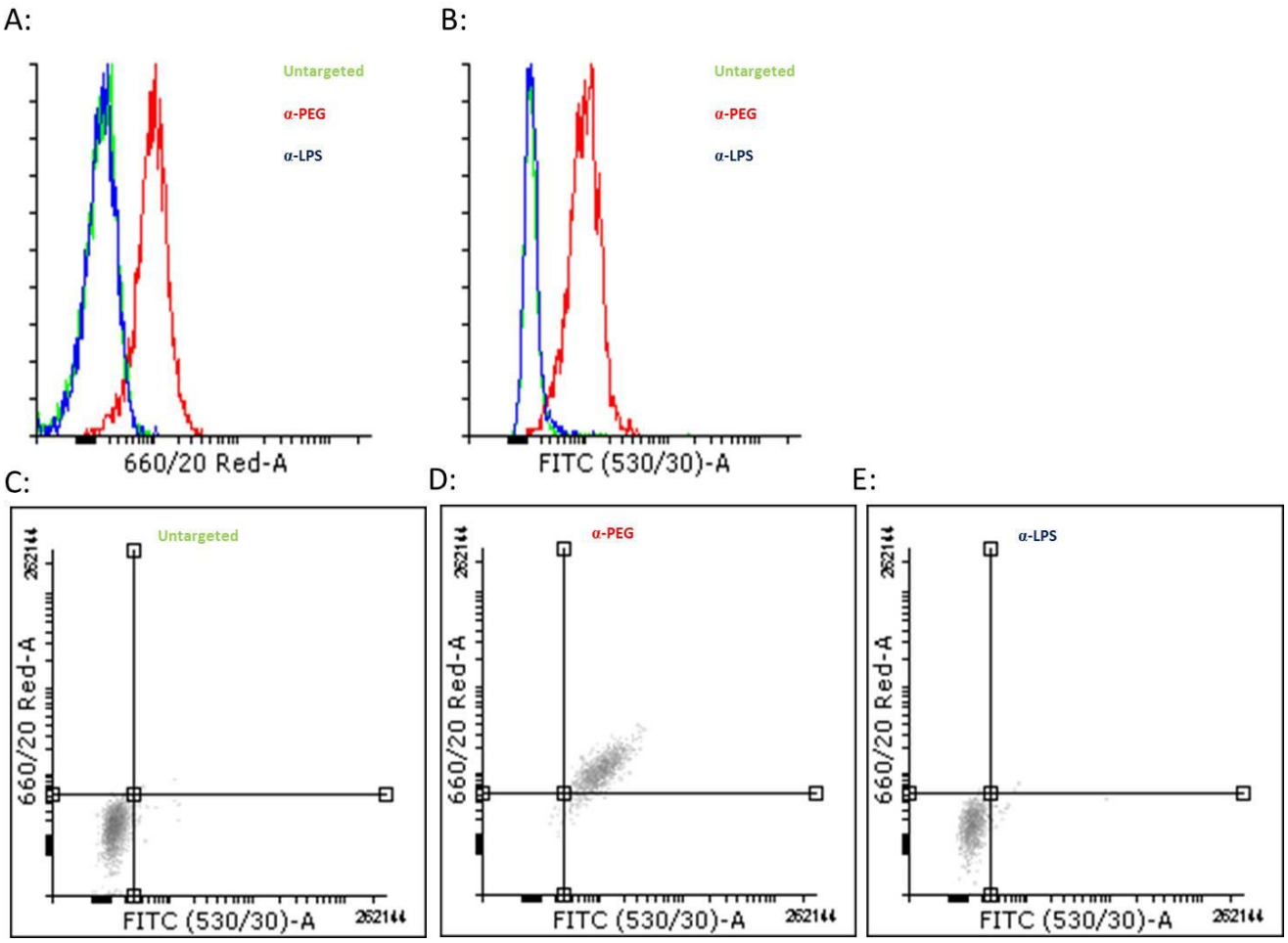

Figure 30: Flow cytometry analysis of anti-EGFR-PEG BsAb mediated co localization of Cy5 labelled PEG nanoparticle.

MDA MB 468 cells were grown to confluency in Advanced RPMI 1640 medium supplemented with 1x Glutamax and 10% FCS and then scraped. Cells were then incubated for 1 hour on ice with either: Cy5 nanoparticle and anti-c-myc FITC (Untargeted); Cy5 nanoparticle, anti-c-myc FITC and anti- EGFR-PEG(15-2) BsAb (anti-PEG); or Cy5 nanoparticle, anti-c-myc FITC and anti-EGFR-LPS BsAb (anti-LPS) in PBSFCS (PBS + 10% FCS). Following incubation, cells were washed with PBSFCS to remove unbound antibody and nanoparticle. Fluorescence was then assayed using a BD LSR II Analyser and data was analysed using Flowing 2.1. Panel A (Count / Absorbance 660nm) shows a shift in Cy5 fluorescence, in the presence of our BsAb and Cy5 nanoparticle, but not with the Cy5 nanoparticle alone or with the anti-EGFR-LPS BsAb and the Cy5 labelled nanoparticle. Panel B (Count / Absorbance 530nm) shows that additional to the Cy5 fluorescence, a shift in fluorescence associated with an FITC fluorophore can be detected in the presence of our anti-EGFR-PEG BsAb Cy5 nanoparticle and an anti c-myc – FITC antibody. Panel C (Absorbance 660nm / Absorbance 530nm) shows no shift in Cy5 or FITC fluorescence. Panel D (Absorbance 660nm / Absorbance 530nm) shows a shift in

Cy5 or FITC fluorescence in the presence of our anti-EGFR-PEG BsAb. Panel E (Absorbance 660nm / Absorbance 530nm) shows no shift in Cy5 or FITC fluorescence in the Presence of an anti-EGFR-LPS BsAb. This supports our hypothesis that interaction between MDA MB 468 cells and nanoparticle are mediated by our BsAb.

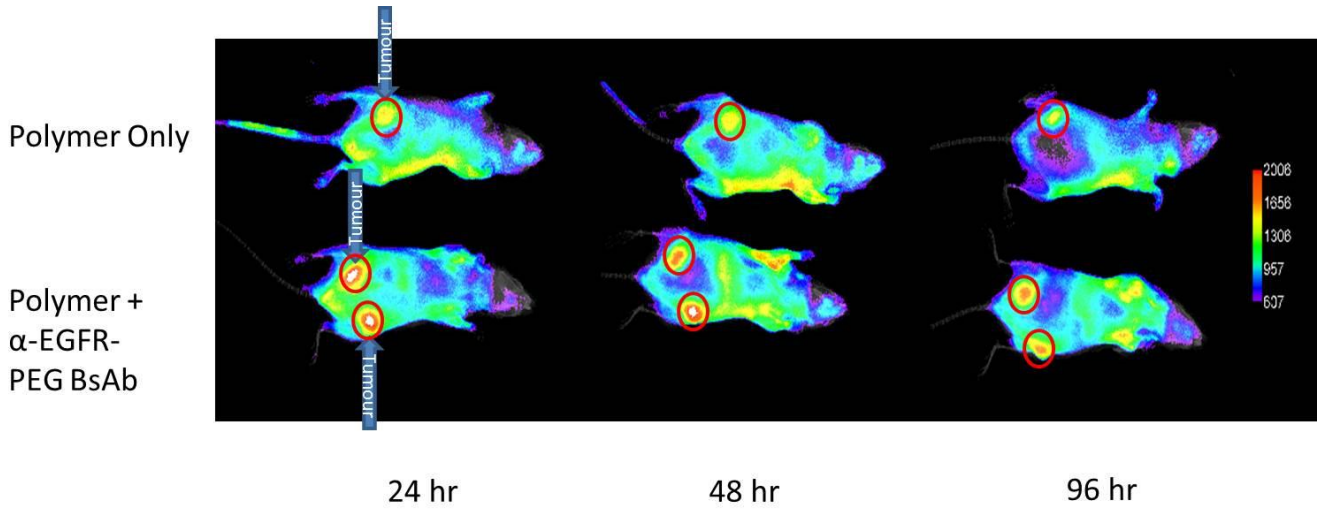

Figure 31: Fluorescence in vivo imaging of MDA MB 468 xenografts in nu/nu mice.

Cy5 fluorescence imaging of MDA MB 468 xenograft mice (tumours circled in red) 24 hrs, 48 and 96hr post lateral tail vein injection with PEG Cy5 labeled nanoparticle and anti-EGFR anti-PEG BsAb dorsal view. Tumours of mice injected with BsAb and nanoparticle show both increased initial exposure of the tumour to the nanoparticle (at 24hrs) as well as significantly increased retention of the nanoparticle within the tumour (96hrs).

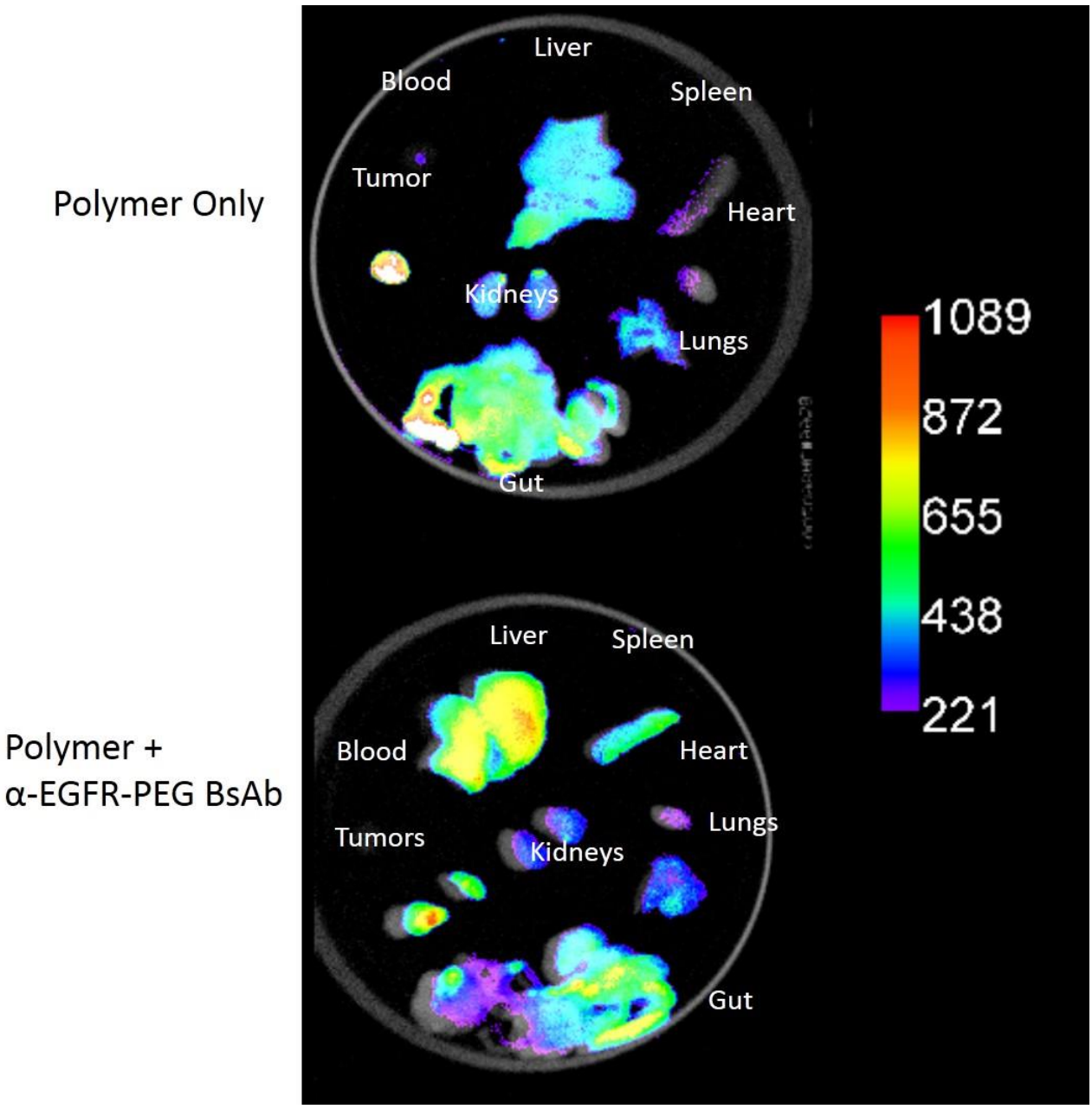

Figure 32: Fluorescence imaging ex vivo of tissue 96 hrs post lateral tail vein injection.

Cy5 fluorescence imaging of organs *ex vivo* from MDA-MB 468 xenograft mice 96hr post lateral tail vein injection with PEG Cy5 labeled nanoparticle and anti-EGFR-PEG BsAb. After 96 hours the nanoparticle is fully cleared from blood when injected as a mixture of BsAb and nanoparticle. However, there is a significant presence of nanoparticle within the tissues of the liver and spleen.